The distribution of sediment residence times at the foot of mountains and its implications for proxies recorded in sedimentary basins

Sebastien Carretier, Laure Guerit, R. Harries, Vincent Regard, P. Maffre, Stéphane Bonnet

The distribution of sediment residence times at the foot of mountains and its implications for proxies recorded in sedimentary basins

June 5, 2020

S. Carretier[1*], L. Guerit[1,2], R. Harries[3], V. Regard[1], P. Maffre[4] and S. Bonnet[1]

[1] GET, Université de Toulouse, IRD, UPS, CNRS, (Toulouse), France.
[2] Now at University of Rennes, CNRS, Géosciences Rennes, UMR 6118, France.
[3] Research Center for Integrated Disaster Risk Management (CIGIDEN), PUC, Santiago, Chile.
[4] Department of Earth and Planetary Science, University of California, Berkeley

[*] Correspondance: sebastien.carretier@get.omp.eu

Abstract

The geochemical and physical properties of terrigenous sediment stacked in sedimentary basins are used as proxies for the paleo-environmental conditions that prevailed during their period of deposition. Nevertheless, sediment grains have a stochastic transit from mountain sources to sedimentary basins: a fraction of grains are stored for a long time while others are recycled from old deposits. Consequently, the temporal representativity of a population of grains in a sedimentary stratum is uncertain. The potential recycling of old material is a major concern in the reconstruction of paleo-environments and this recycling is usually difficult to evaluate. In particular, the distribution of grain residence times in basins, between sources and sinks, is out of reach. Here we use a landscape evolution model that traces grains to analyse the distribution of residence times in an alluvial apron at the foot of a mountain relief. We study an end-member scenario that is the least favourable for the storage of grains: when the mountain is eroding at the same rate as rock is uplifting. In this case, the alluvial apron behaves as a by-pass zone, when averaging sediment flux over Ma, and the storage of grains of any size should be minimal. Yet, the model predicts that some grains are stored for hundreds of thousands of years before exiting the alluvial apron. Consequently, the mean residence time of sediment grains is much higher than the observed residence time of 95% of the grains exported by the alluvial apron rivers. This process may explain very long residence times found in fluvial systems by geochemical methods based on bulk measurements of sediment. Furthermore, it suggests that grains stored for a very long time, although a minority, can bias time-dependent proxies.

Keywords: Grain, residence time, piedmont rivers, paleo-environmental proxy, landscape evolution modelling.

1 Introduction

The fate of terrigenous sediment is to be stacked in sedimentary onshore or offshore basins, where they often constitute the unique record of paleo-environmental conditions that prevailed during the period of their deposition in stratum. The size, mineralogy and weathering grade of sediment, for example, provide valuable information about changes in tectonic rates (*Duller et al.*, 2010; *Whittaker et al.*, 2011), eroding sources (*Garzanti et al.*, 2007; *Weltje and Brommer*, 2011; *Riquelme et al.*, 2018) or paleo-climate (*Clift and Webb*, 2018). A conventional assumption, which relates the physical and chemical characteristics of sediment with eroding sources for some time period, is that grains are rapidly transported from their source to the basin. However, it is well known that the transport of sediment is highly variable from short timescales (*Einstein, H.A.*, 1937) to long timescales (*Kim and Jerolmack*, 2008; *Paola et al.*, 2009; *Allen et al.*, 2013). In particular, sediment grains can be stored for different periods of time in river bars and terraces (*Allison et al.*, 1998), or in intramontane sedimentary basins (*Jonell et al.*, 2018), as well as in proximal piedmonts and foreland basins. As fluvial erosion processes are highly variable in space and time, either autogenically (*Van De Wiel and Coulthard*, 2010; *Foreman and Straub*, 2017) or because the climate and the production of sediment itself varies, grains that were previously stored can be re-entrained and flushed downstream to distal basins (*Jolivet et al.*, 2014; *Guerit et al.*, 2016; *Malatesta et al.*, 2018). Consequently, grains that were stored for years to millions of years can potentially contribute to the sediment outflux of rivers supplying basins (*Wittmann et al.*, 2011; *Quick et al.*, 2019).

Of primary importance is the long-term storage of grains along the fluvial system. Sediment storage can buffer the transmission of sediment signals from source to sink, such as climatically driven sedimentary signals that are transmitted to basins (*Metivier et al.*, 1999; *Fedele and Paola*, 2007; *Blöthe and Korup*, 2013; *Armitage et al.*, 2013). For example, in the Indus river, about 50% of the sediment outflux to the ocean was recycled from floodplains since the last glacial maximum, masking the effect of monsoon weakening since 8 ka (*Clift and Giosan*, 2014). The storage-recycling process has two potential negative impacts on the reconstruction of paleo-environmental conditions. First, if the proportion of recycled material is high, the bulk property of a stratum may not represent the conditions nor the eroded sources that prevailed at the time of the deposit, but rather a complex mix of previous conditions, possibly smoothing out any source variability. Secondly, if grains stay a long time in traps, their weathering, or any other proxy that depends on mean grain residence times in the fluvial system, will not correspond to the climatic conditions that prevailed during the deposition of a stratum. Such a lag has been identified, for example in South China Sea, where the onshore Holocene sediment record reflects chemical weathering during the last glacial maximum (*Hu et al.*, 2012). The magnitude of recycled sediment is usually unknown in old deposits and this issue has been identified as a major potential bias for high resolution records that utilise the mean (bulk) property of a sediment sample (*Di Giulio et al.*, 2003; *Weltje*, 2012; *Hoffmann*, 2015).

Indeed, there are data that suggest that the storage of sediment can be long even for very fine sediment. Disequilibria between isotopes of Uranium-series ($^{234}U/^{238}U$ *Chabaux et al.*, 2006; *Li et al.*, 2016a) have been used to determine a "comminution age" of sediment, defined as the time elapsed between the generation of small grains ($\leq$ 50 μm), by any process in the source region (local weathering in the regolith, crushing during river transport), and the length of time that the deposit spent at the sampling location. The comminution age is an age that is supposed to represent a mean transit time of all the grains constituting a sample. Very long comminution ages of 110 kyr and 250 to 600 kyr were found in sediment currently being transported along rivers in Taiwan, and along a river draining the east of the Tibetan edge, respectively (*Li et al.*, 2016a). These long comminution ages, and the absence of a strong correlation with the "Chemical Index of Alteration" (CIA), which measures the depletion in alkalis of sediment grains by weathering, suggest long-term storage in the fluvial system and the reworking of older sediment. Other examples of long and variable comminution ages (18 to 650 kyr) include large catchments draining into the Gulf of Carpentaria in northern Australia (*Martin et al.*, 2019). Uranium-series disequilibria were also used for evidence of residence times of a few kyr in the Amazon basin (*Dosseto et al.*, 2006) and $\sim$ 100 kyr in the Gange plain (*Granet et al.*, 2007) for fine sediment ($\leq$ 50 μm). In addition, *Wittmann et al.* (2011) used cosmogenic nuclides as evidence for the recycling of old sand ($\leq$ 125 μm), stored in the Amazonian plain, by the current river. *Lauer and Willenbring* (2010) also showed that the recycling of sediment deposited in the floodplain is likely to lead to a downstream increase in the mean river sand cosmogenic nuclide concentration. Using detrital apatite fission-track thermochronology on sediments from rivers in New Zealand, *Lang et al.* (2018) demonstrated the importance of intermontane sediment storage over timescales of 10 to 100 kyr. All these studies point to long ($>>$ 1 kyr) temporary storage of fine sediment, even in rapidly eroding landscapes.

Coarse sediments are transported as bedload, more slowly than fine sediment, and with a higher probability of being trapped in deposits (*Fedele and Paola*, 2007). Alluvial rivers move laterally over decennial to millennial timescales, either by slow lateral erosion in meandering rivers, through the constant reorganization of channel connections in a braided river, or by abrupt deviation from a former course (avulsion) during extreme floods. During this lateral migration of channels, bedload sediments are abandoned for different periods of time (storage) and can be re-entrained, years to million of years later, when a channel reoccupies this former position (recycling). For example, a recent study used the distribution of cosmogenic nuclide ^{21}Ne in distinct pebbles in the Great Plains (USA) to infer that the current river is recycling Mio-Pliocene sediment (5 Ma old) (*Sinclair et al.*, 2019). In a canyon of the Western Andes, *Carretier et al.* (2019) measured the ^{10}Be in distinct pebbles from a known source to show that storage and recycling control the rate of dispersion of river pebbles over the long-term. Yet, because the alluvial processes involved in the storage and recycling of fine and coarse sediments are diverse and operate over a wide range of timescales, both the distribution of grain residence times and the amount of sediment recycling through time is poorly known (*Allison et al.*, 1998; *Bradley and Tucker*, 2013).

In this contribution, we use a numerical model of topographic evolution over geological timescales (landscape evolution model) that traces grains to study the relationship between the processes controlling storage and recycling and the resulting distribution of grain residence times in an alluvial apron, refered to as a piedmont. We restrict our analysis to a piedmont system because it is the most proximal area of sediment deposition and remobilisation, between mountainous sources and distal long-term sedimentary basins, with a high potential of storage (*Fedele and Paola*, 2007; *Harries et al.*, 2019).

2 Modelling Approach

We use the landscape evolution model CIDRE (see details in Appendix A and in *Carretier et al.*, 2016, 2018). CIDRE models the topographic evolution of a fluvial landscape on a regular grid of square cells. Starting from an initial topography, the modification of the topography proceeds in successive time-steps. Over a time-step, a specified precipitation rate falls on the grid and a water discharge is propagated from the most elevated cell to the lowest cell. In each cell, local erosion and deposition rates are calculated according to laws that depend on the local water discharge, topographic slope and a transport length parameter that determines the mean distance that a sediment particle must travel before being deposited. In addition, rivers can erode laterally and the lateral erosion is proportional to the sediment discharge in the river. An originality of CIDRE is that it includes individual grains, allowing the paths of sediment to be traced from their source to their sink. The grains have specified sizes and initial positions within the grid and at depth. The size of grains does not change downstream and the grains are not split into different smaller clasts. Grains then move stochastically according to probability laws that depend on the local erosion and deposition rates (*Carretier et al.*, 2016). The movement of grains is thus consistent with the topographic modifications calculated by CIDRE (*Carretier et al.*, 2016).

The simulations consist of a block of 40x60 km^2 that uplifts at a constant rate of 1 mm yr^{-1} to reach a dynamic equilibrium between erosion and uplift. This uplifting block is coupled to a deposition area of 40x60 km^2, where sediment accumulates until reaching a by-pass stage, without the influence of subsidence (Fig. 1 and see Appendix A for parameter values). The precipitation rate varies spatially and temporarily with elevation according to a Gaussian-like function of precipitation rate versus elevation (*Zavala et al.*, 2020), such that the precipitation rates vary from 1 m yr^{-1} at baselevel to a maximum of 1.7 m yr^{-1} at 1300 m, a peak elevation usually found in Himalaya or Andes (*Bookhagen and Burbank*, 2006; *Bookhagen and Strecker*, 2008; *Colberg and Anders*, 2014). In these dynamic equilibrium and by-pass conditions, the storage of grains in the alluvial apron is less likely, as any grain entering the piedmont will leave it at some time. Yet, we will show that long-term storage still occurs. This model is idealistic and does not intend to reflect a specific field location. We study this end-member model because it is useful to understand the processes that dictate sediment storage and recycling. We begin by analyzing the autogenic incision and lateral migration of rivers in the model. Then we spread, at the surface of the model, a population of gravels (1-10 cm in diameter) to analyse how these grains can be stored or leave the model grid, and further, how their residence times (the duration between entry and exit from the piedmont) are finally distributed. In a second series of simulations, we continuously feed the piedmont with grains and trace their ages (time since their entry in the piedmont) in the piedmont and their residence time once they have left the model grid. This allows us to evaluate the impact of "old" recycled grains on the mean age and mean residence time, through time, and finally to discuss the natural variability in residence-time-dependent proxies in basins.

Only some of the model parameters are likely to have an impact on the results of this study. These parameters are those that control the river erosion and sediment dynamics in the piedmont domain (Appendix A): the exponents m and n on the water discharge and slope in the sediment erosion law, which dictate how the detachment rate of sediment varies with water discharge and slope; the transport length parameter ζ that determines the length of transport of sediment entering the piedmont domain (higher ζ means less deposition and longer travel); the lateral erosion coefficient α that controls part of the lateral mobility of piedmont rivers (higher α means more intense lateral erosion). In addition, the piedmont length perpendicular to the mountain front may influence the probability of temporary storage and the precipitation rate may also affect the river dynamics in the piedmont. The model time-step used to solve the equations can also influence the non-linear dynamics of river movement on the piedmont and the grain dispersion (*Carretier et al.*, 2016). We will test the effect of varying all these parameters on the residence time distribution of grains in the piedmont. All other parameters (erodibility parameters in particular) may affect grain elevation within the mountain domain, but as the duration of grain transport in the mountain domain is not studied here, these parameters will not influence the outcomes presented in this contribution.

3 Results

3.1 Dynamic equilibrium

In order to understand the distribution of grain residence times, we run the model during 20 m.y. and analyse the model behaviour at dynamic equilibrium. A 20 m.y. duration ensures that the observations are not due to sedimentation that would keep on increasing during the transient adjustment to uplift (Fig. S1). From this situation, the model time is set to zero and the model maintains dynamic equilibrium for the succeeding 5 m.y. Fig. 2a and b show two snapshots of the model topography with the water discharge overlain. One million years separate the two snapshots and there is, indeed, no noticeable difference in the mountain part. However, the fluvial pattern in the piedmont is different. The erosion/sediment rate pattern (Fig. 2c and d) shows that sedimentation occurs along main piedmont rivers on levées and lobes. The interplay between sedimentation and erosion, as well as the lateral erosion of rivers, generate continuous lateral river migration as well as abrupt avulsions and captures, so that the deposition and the storage of material are episodic. Although the mean cross-range profile is constant over time (Fig. 2e), the transverse profile of the piedmont shows topographic variations of 60 m associated with the autogenic alluvial dynamics (Fig. 2f). Furthermore, the mountainous domain is not eroding uniformly: there are zones with sedimentation, and channel reaches with focused erosion. Fig. 3 illustrates successive steps over 500 kyr. Autogenic incision of the piedmont apex occurs naturally in these experiments, preferentially when two rivers join in the piedmont (Fig. 3a). Incision at alluvial fan apexes drives small knick-points that retreat upstream, generating a pulse of sedimentation in the piedmont (Fig. 3b-f) that favours avulsions and increases the probability of channel captures. Thus there is a positive coupling between the dynamics of the mountain and the piedmont. In summary, although a steady-state equilibrium can be defined macroscopically with 1) a constant mean long-profile from the mountain to the piedmont, 2) a constant mean erosion in the mountain and 3) by-pass of the piedmont over long timescales (Fig. S1), this equilibrium is imperfect and high frequency topographic variations ($\sim$ 100 kyr) still occur (Fig. 2e). This is fundamental to understand the distribution of grain residence times in the piedmont.

3.2 Tracing one population of grains

We now randomly spread 10,000 grains at the surface of the mountain domain at time 0 and we track their pathway during 1 m.y. of model time. The grain size is distributed uniformly between $r = 1$ cm and 10 cm. Fig. 4a shows that most of the grains are rapidly evacuated from the model domain but some grains are stored in the piedmont. $> 95\%$ of the grains were stored less than 400 years in the piedmont, but a minority of grains ($< 1\%$) reached residence times approaching 1 m.y. (Fig. 4b). The mean residence time is 18 ka, one order of magnitude larger than for most of the grains. The long tail of the distribution is illustrated by the complementary cumulative distribution for different selected grain sizes in Fig. 4c. On this figure, we also added an experiment with 10,000 grains of a constant grain size of 1 mm, representative of a coarse sand fraction. This figure shows that gravel of different sizes have similar residence times whereas small grains of 1 mm have consistently lower residence times (mean of 2.8 kyr), resulting from their higher probability to be entrained ($\propto 1/r$ in the model). The tail of the distribution may be approached by a power law between 10 and 100 kyr, whereas an exponential decline may be more appropriate for longer durations. Given the difficulty in proving a power-law trend (*Virkar and Clauset*, 2014), we did not attempt to fit our distributions. Rather, we show different reference slopes in Fig. 4c and in subsequent figures to qualitatively evaluate the length of the tail (the smaller the slope in the log-log plot the longer the tail, and thus old grains are more probable). The abrupt exponential cut-off for durations > 100 kyr, results from the fact that the grains must leave the system at some moment, infinite storage is unlikely given the by-pass stage of the piedmont and the absence of subsidence.

The long-term storage of some grains is explained by episodic sedimentation, as described in Fig. 3. Most of the grains leave the piedmont in several model time-steps (< 400 yr in the reference model). Nevertheless, some grains are deposited on river sides and can stay there for a long time before being recycled by an avulsion event or by the more continuous lateral migration of rivers.

Considering a grain population of 1 to 10 cm, we vary some of the parameters that likely influence the residence time and then compare their complementary cumulative distributions to the previous model, taken as reference (Fig. 5). As expected, doubling the piedmont length increases the residence time (mean $\sim$ 50 kyr) and dividing the piedmont length by two decreases the residence time (mean $\sim$ 5 kyr). The probability of a grain being stored in a river deposit increases with piedmont length. The mixing layer has the shape of a wedge in the downstream direction. It scales with the square of the piedmont length, and thus so does the mean residence time. Consequently, the mean residence time strongly decreases when the piedmont length decreases. A model time-step, ten-times smaller, decreases the fraction of grains that leave the model rapidly, but increases the fraction of grains stored for a long time, thereby having a lesser impact on the mean residence time (mean $\sim$ 23 kyr). Multiplying the transport length parameter ζ by a factor of 4 predictably decreases the residence time (mean $\sim$ 10 kyr), because a larger ζ decreases the probability of grain deposition. Doubling the lateral erosion efficiency α has a limited impact (mean $\sim$ 18 kyr), suggesting that abrupt changes in a river's course, through avulsions and captures, have a stronger influence than their continuous lateral migration. Changing the exponent m from 0.3 to 0.5 for water discharge in the sediment erosion law (corresponding to a lower daily variability of piedmont rainfall for example *Lague*, 2014) decreases drastically the residence time (mean $\sim$ 2 kyr). With $m = 0.5$, the piedmont is more gentle, the piedmont rivers move much less laterally and thus topographic variations in the piedmont are reduced. The rivers export sediment out of the model domain more efficiently, and thus grains have a smaller probability of being stored in lateral deposits. Dividing the precipitation rate by two increases the mean residence time (mean $\sim$ 30 kyr). Despite all of these different reference model scenarios, in all cases, we observe that the distribution of residence times has a long tail, i.e. a small but still probable proportion of grains with very large residence times.

3.3 Distribution of grains ages and residence times through time

In order to analyse the evolution of the mean residence time through time, we now use 200,000 grains (1-10 cm) and visualise them as they progressively cover the piedmont. When grains leave the model domain, the time they spent in the piedmont (residence time) is recorded. To compensate for the depopulation of grains in the mountains, the grains leaving the models are repositioned in their original position in the mountain and their clock is reset to zero.

We track the grains movement during 5 m.y. Consistent with "Reservoir Theory", we differentiate the "age" of a grain from its "residence time". The age applies to grains still in the piedmont and corresponds to the time elapsed since their entrance in the piedmont. The residence time applies to grains leaving the piedmont, is thus necessarily longer for a given grain, and corresponds to the total time elapsed between the entrance and the exit of a grain. In the two snapshots of Fig. 6, young grains together with grains as old as 1 Ma or more are present at the surface, but the spatial repartition of ages is different in each snapshot, highlighting a constant reworking of the piedmont surface. Grains of similar ages are grouped in different zones that correspond to different, successive sedimentary lobes. Fig. 6c thus demonstrates that older grains are not older because they are buried deeper in the lobes. Rather, for a given age, grains are buried relatively equally between 60-70 m and the surface, i.e. within the long-term mixing layer, identified on Fig. 2e. Fig. 6d demonstrates that the distribution of grain ages at 3.75 m.y. in the mixing layer is spread between a few years and >2 Ma (histogram truncated at 2 Ma).

The age distribution is different from the distribution of residence times. Fig. 7a shows the evolution of mean ages for different models (reference, longer and shorter piedmont, higher ζ, higher α). In the reference model, the mean age increases and reaches 0.8 Ma after 5 Ma of evolution (Fig. 7a). This increase highlights the fact that the number of old grains increases through time. Nevertheless, the increase is not infinite, as grains must leave the piedmont at some point in the "steady-state" simulations. The mean ages saturate after 5 Ma (not illustrated), which is interpreted as the time needed to completely rework the piedmont mixing layer. We observe similar behaviours with the other models. Variations in piedmont length have a limited impact on this mean age whereas increases in the other two parameters tested here, ζ and α, leads to a significant decrease in the mean ages: a larger ζ decreases the probability of grain deposition and a higher α favours the lateral re-entrainment of stored grains (Fig. 7a).

In order to analyse how the mean residence times of grains leaving the piedmont varies through time, we calculated every 10 kyr, the mean residence time of grains that left the model during a model time-step (10 yr). In the reference model, the mean residence time is highly variable between several centuries and 80 kyr (Fig. 7b). This variation communicates the stochastic recycling of grains of different ages. Even if most of the grains travel fast, the incorporation of old grains will strongly affect the mean. Longer piedmonts have larger variations in residence time, although the mean age is not very different from that of the reference model (Fig. 7a and b). The probability of recycling old grains is larger for long piedmonts, which explains these variations. Consistently, a smaller piedmont leads to smaller variations (Fig. 7b). Doubling the lateral erosion efficiency increases the variability of mean residence time because lateral erosion increases the probability of recycling grains along the river course (Fig. 7c). On the contrary, increasing the transport length parameter ζ increases the fraction of grains that travel fast, and thus decreases the variations of the mean residence time (Fig. 7c).

We expanded the period of observation by collecting all the exiting grains during one hundred consecutive time-steps (i.e. during a period of 1000 years), then calculated their mean residence time and compared the results with previous estimates. Fig. 8 shows that the variability in residence time is reduced but still significant, and that exceptional large peaks still occur. This variability thus appears to be consistent irrespective of the time scale, the size of the system and the values of the parameters.

It is interesting to compare the mean age and residence time with the predicted turnover time in the piedmont. The turnover time is the duration needed to remove a population of grains from the piedmont. In Reservoir Theory, this time is the ratio of the total volume of the reservoir over the outgoing flux (in L^3 T^{-1}). This time is often used to characterise the "mean" residence time of a particle in a natural reservoir. When this reservoir is perfectly mixed and at steady-state (influx=outflux), the predicted distributions of the grain ages and residence times are exponential and their mean values are equivalent to the turnover time (*Mudd and Yoo*, 2010). In our case, the reservoir volume is the surface of the piedmont multiplied by the mean depth of the mixing layer, estimated at $\sim$60 m in the reference model. The outgoing flux is simply the mountain area multiplied by the uplift rate (1 mm yr^{-1}). The resulting turnover time is $\sim$60 kyr. The turnover times of the different models are plotted as dashed lines of the same color as both the corresponding age and residence time evolutions in Fig. 7. The mean age diverges and greatly exceeds the turnover time, whereas the mean residence time is smaller. The turnover time is thus a very poor and incorrect metric of the mean time spent by grains in a sample taken at the outlet of the piedmont. *Bradley and Tucker* (2013) gave a comprehensive explanation of this difference in the case of a meandering river. They proposed that the mean age strongly exceeds the turnover time because the probability to erode old deposits stored on the borders of the valley-floor is smaller than the probability to erode young deposits present near the center of the valley. A similar reason applies to the piedmont case: old deposits are located in topographic highs or far away from main rivers, so that they are mostly recycled during the rare passage of an avulsing river. The mean residence time is much smaller than the turnover time because most of the outgoing flux of grains are those that were conveyed very fast in a river, from their entry point in the piedmont to their exit. The perfect mixing model is thus inappropriate here.

4 Discussion

4.1 Realism of alluvial dynamics

Qualitatively, the model reproduces a variety of geomorphic features also observed in natural settings (*Bernal et al.*, 2011): levées, splay-offs, continuous migration of channels by lateral erosion, sudden avulsion by upstream deviation or by river capture.

The decreasing sedimentation rate in a direction perpendicular to a channel, as seen in Fig. 3 has been documented, for example, along a portion of the Brahmaputra (*Allison et al.*, 1998).

In laboratory experiments of alluvial fans, superimposed on variations linked to changes in water influx and base level, a cyclic pattern of incision and deposition is always observed, (*van Dijk et al.*, 2009; *Clarke et al.*, 2010; *Reitz et al.*, 2010; *Powell et al.*, 2012) where this autogenic behaviour is related to lateral erosion and fluvial avulsions, as observed in natural settings (*Field*, 2001). Several field studies recognize clustering of fluvial paleo-channels as the stratigraphic expression of autogenic fluvial processes related to fluvial migration and avulsion (*Hajek et al.*, 2010; *Hofmann et al.*, 2011; *Hajek et al.*, 2012; *Flood and Hampson*, 2014), as observed in the simulations.

Furthermore, we observe autogenic entrenchments at fan apexes and an associated retreating erosion wave in the mountain rivers, which is also observed in laboratory experiments of alluvial fans (*Schumm et al.*, 1987; *Reitz and Jerolmack*, 2012), in numerical models (*Humphrey and Heller*, 1995; *Carretier and Lucazeau*, 2005; *Wang et al.*, 2011) and in the field (*DeCelles et al.*, 1991; *Giosan et al.*, 2012). A direct consequence of this behaviour is a cyclic variation of the slope around the mean value, which can reach up to 10% (*Kim et al.*, 2006; *van Dijk et al.*, 2009), in agreement with field observations (*Kim et al.*, 2006). Scaled to our numerical piedmont, this would induce a variation in elevation of up to 80 m, consistent with the observed 60 m layer of reworking.

It is difficult to compare more quantitatively our simulations with other experiments or natural examples, in particular concerning the frequency of avulsions, or floodings in the piedmont (*Reitz et al.*, 2010). Indeed, the alluvial dynamics in the piedmont seems intimately linked with the dynamics of erosional waves in the mountain, but laboratory experiments coupling mountain and piedmont are sparse (*Schumm et al.*, 1987; *Babault et al.*, 2005; *Rohais et al.*, 2012) and have not yet analysed this aspect. These phenomena occur over tens of thousands of years and are thus very difficult to document in the field (*Bekaddour et al.*, 2014).

4.2 Could the long-tailed distribution of residence times be the result of a bias in our modelling choices?

4.2.1 Transport parameter

In a cell, erosion and sedimentation are dependent on a ζ transport parameter; the larger the ζ, the lower the deposition rate and the lower the probability of having long grain residence times. Indeed, simulations using a value of ζx4 generate lower residence times, however, it must be recognised that the residence time distribution always shows a long tail with a mean much higher than the 95% residence time of the grains (Fig. 5). An infinite ζ value would not be realistic in alluvial domain because there would be no deposition. The case where ζ is infinitesimal would increase deposition and thus the probability of storing sediments over long periods of time.

4.2.2 Lateral erosion

Lateral erosion is also poorly constrained in landscape evolution models. While other lateral erosion laws have been used (e.g. *Hancock and Anderson*, 2002), lateral erosion appears to have a minor role on grain storage over long periods in our simulations where storage occurs mainly due to avulsions and captures. This is confirmed by similar results obtained for two simulations with two differing values of α (Fig. 5). An additional simulation that does not account for lateral erosion results also in a long-tailed residence time distribution ($\alpha = 0$, Fig. S2). We therefore conclude that the parameterization of lateral erosion should not bias our conclusions.

4.2.3 Erosion law

Our simulations show that the choice of erosion law has a very large influence on the lateral mobility of rivers and thus on residence times: A slight increase in the exponent of the power law between the detachment rate and the flow rate (0.3 to 0.5) drastically decreases residence times (Fig. 5). Rivers become less mobile such that grains leaving the mountain are exported more quickly from the foothills, while still maintaining a residence time distribution with a long tail due to the storage of some grains for long time periods on alluvial fans. This exponent is likely also dependant on variations in water discharge and grain size (e.g. *Deal et al.*, 2017). Although a constant and homogeneous value is simplifying, it does not seem to artificially introduce a residence time distribution with a long tail.

4.2.4 Grain size

Another important simplification is the absence of downstream change in grain size. The importance of coarse grains in influencing channel mobility under variable sediment and water discharges was recently demonstrated experimentally (*MacKenzie and Eaton*, 2017). The downstream sediment fining in basins also leads to changes in alluvial dynamics perpendicular to the range: the more distal transition to meandering rivers (*Dingle et al.*, 2020) is not taken into account in Cidre. Similarly, the existence of a transport threshold in the detachment law, which can modify the slope of the fans (*Parker et al.*, 1998) and the alluvial dynamics, remains to be evaluated. We anticipate, however, that an erosion threshold would increase the heterogeneity of erosion on the foothills and thus would favour the storage of certain grains for long periods.

4.3 Does the grain displacement algorithm influence the residence time distribution?

Carretier et al. (2016) verified that the mean and standard deviation of grain displacement were consistent with the calculated sediment fluxes. The dispersion of grains displaced by purely gravitational processes (without water entrainment) is, however, overestimated (*Carretier et al.*, 2016), but these phenomena are negligible on the piedmont. There is also a simplifying assumption that the probability of grain detachment is inversely proportional to size and not to deposition. If the probability of deposition increased with grain size, there would be more large grains with long residence times, which would be in line with our conclusions. Furthermore, simulations with a single grain size do show a long-tailed residence time distribution (Fig. 4). We therefore conclude that the choice of probability law to move the grains does not artificially bias the shape of the residence time distribution.

Despite these limitations, we consider that our main findings can be confidently extrapolated to the real world. In all of our simulations, we observed long-tailed distributions of residence times. There is thus a significant probability for grains, which were once stored for a long time in former deposits, to be recycled. The reasons for such long-term storage are well-identified: Deposition is episodic and the probability of eroding previous deposits is lower for older deposits than for younger deposits. Episodic deposition occurs due to levées, splay-offs, lobes, avulsions and captures, and their autogenic feedbacks with erosional waves in the mountain. The lower probability of eroding older deposits is a simple geometrical problem (*Bradley and Tucker*, 2013): old deposits are topographically higher or distant from active rivers after an avulsion. Their long-term preservation, achieved by avoiding erosion, is the reason why they are so old. If the probability of erosion was homogeneous in the piedmont, the piedmont would have a much thinner distribution of younger ages. Thus, although the absolute value of residence times can vary between models and the real world, the prediction of long-term storage is a robust result.

4.4 Departure from equilibrium

In nature, mountain front systems are usually out of equilibrium, contrary to the simulations presented here. In natural systems with active subsidence, like the Pyrenees during the Eocene, the Bolivian Andes during the Neogene or the Apennines in recent times, very old grains would not be found in the mixing layer at the basin surface because these grains would be buried deeper. Storage and recycling would occur within the piedmont mixing layer, potentially leading to a long tailed-distribution of residence times, but with a much smaller range of times. The maximum age of grains found at the piedmont surface will depend on the ratio between the subsidence rate and the reworking rate of the mixing layer ($\sim$ 60 m in our simulations).

At the beginning of an orogeny, when the subsidence rate is rapid with a Flysch stage, the reworking rate is small compared to the subsidence rate. In our simulations, the time needed to rework completely the piedmont surface is $\sim$ 5 m.y. If a basin subsides at 0.25 mm yr^{-1} for example, grains are buried below 1.25 km in 5 m.y. Only grains of several thousand years in age can be present at the surface (see supplementary Fig. S3).

On the contrary, when the mountain range approaches a dynamic equilibrium, as could be the case in some portions of New Zealand or Taiwan (*Hovius et al.*, 2000), the subsidence rate decreases and grains as old as several m.y. can be recycled at the surface of the piedmont. Recycling can take place in the forebergs that exhume sediments, like in the Siwaliks (*Quick et al.*, 2019) or directly on the surface of the foothills, as in our simulations. This phenomena can be amplified if a climate change drives a flexural rebound of the range and its foreland, exhuming old sediment by river incision, as proposed for the Himalaya foreland (*Burbank*, 1992).

Finally, in the post-orogenic stage, previously buried sediment is exhumed and can be recycled into the flux of sediment exported to distal basins, with grains potentially dating back to the Neogene (*Tucker and van der Beek*, 2013). This is the case in the Great Plains, USA (*Sinclair et al.*, 2019) and the European Alps (*Cederbom et al.*, 2004). The probability of recycling old grains must, therefore, vary during the orogenic cycle. We anticipate that this probability could be formalised as proportional to the ratio $H/\dot{S}\Delta t$ where H is the reworking or mixing layer, $\dot{S}$ is the sedimentation rate and Δt is the time needed to rework all of the foreland surface.

Climate variability also drives fluctuations in the erosional flux from mountain ranges over geological timescales (e.g. *Clift*, 2006; *Goodbred and Kuehl*, 2003). Over the Quaternary, entrenchment and aggradation are often associated with shifts in climate and sea level (e.g. *Bekaddour et al.*, 2014; *Ganti et al.*, 2016; *Malatesta et al.*, 2018). These behaviours likely influence the degree of sediment recycling. For example, when rivers incise into their former deposits, they first recycle a large amount of previously stored grains, but once constrained between their valley walls, the recycling may become a minor component. This variable degree of recycling during entrenchment is illustrated by a recent study based on Optically Stimulated Luminescence (OSL) data of a large population (> 100) of individual grains. Along a New Zealand river, *Bonnet et al.* (2019) document an overestimation of the age of fluvial deposits, up to order of magnitude, when a bulk mean OSL age is considered. Interestingly, however, they also demonstrate that the magnitude of the age overestimation, depending on the tail of the single grain distribution, is primarily influenced by the incision rate of a river, through its control on sediment supply from the hillslopes to the river. In addition, when rivers aggrade, their lateral mobility increases (*Reitz and Jerolmack*, 2012; *Bufe et al.*, 2016), favouring recycling. It is thus predicted that the degree of recycled sediment varies across climatic cycles but temporary grain storage in valleys or on alluvial fans, as shown in our simulations, should still occur.

4.5 Implications for proxy in sedimentary basins

Our results show that the recycling of very old grains has a strong influence on mean residence times, which can be orders of magnitude higher than the residence time of 95% of transported grains. Our study complements recent evidence of storage in intramontane domains (*Lang et al.*, 2018; *Jonell et al.*, 2018), in arid river valleys (*Giosan et al.*, 2012; *Carretier et al.*, 2019) and in simulated floodplains (*Bradley and Tucker*, 2013) (Fig. 9). Consequently, any proxy that depends on the residence time of sediment and which is determined from a bulk measurement of a sediment sample, can be affected by recycled grains.

Although our simulations were carried out with coarse sediment, the identified causes for long storage and long tailed distributions of residence times likely apply to fine sediment as well. For example, this age amplification effect may partly explain the very old comminution times of several hundreds of thousands of years found for very fine sediment in rapidly eroding mountains like Taiwan or New Zealand. Variations in residence times illustrated by Fig. 8 may also be consistent with the order-of-magnitude difference in inferred comminution ages at the same sampling point in a catchment in the Gulf of Carpentaria, northern Australia, for two dates separated by 8 years (*Martin et al.*, 2019). Although this example is not a piedmont, a long-tailed distribution of residence time, generated by variable recycling in the fluvial system, may explain the observed differences. Comminution times, although useful for quantifying sediment transfer rates, may thus represent a maximum value for the residence time of the majority of grains in a sample.

Other proxies that depend on grain residence times may also be affected, such as the Chemical Index of Alteration. The presence of a minority of old weathered grains in a sample can lead to a high CIA, whereas most of the other grains have a lower CIA. However, weathering rate scales with $t^{\sim -0.4}$ (t time of exposure to weathering - *Gabet and Mudd*, 2009) and long-tailed CIA distributions are therefore less likely. Several studies have shown a correlation between the CIA and other paleo-climatic proxies over periods of millions of years (e.g. *Wang et al.*, 2019) in Asia for the ∼15 Ma monsoon strengthening (e.g. *Clift et al.*, 2008). These consistent variations suggest either a minor effect of the addition of highly weathered grains on these timescales, or the absence of significant additional weathering during storage in the foothills (e.g. *Mondal et al.*, 2012). In other cases, variations in CIA have been found to be uncorrelated with other proxies, such as in the South China Sea where CIA remains unresponsive to monsoon intensification and duration over the last 14 ka (e.g. *Hu et al.*, 2012). The variations of CIA in these cases could correspond to the chaotic recycling phenomena observed in our simulations (e.g Fig. 7). For offshore basins, delta dynamics may also transform the sedimentary signal (*Li et al.*, 2016b; *Foreman and Straub*, 2017) and influence the residence time distribution of deposited grains, which remains to be assessed.

As the recycling process is stochastic, Figs. 7 and 8 show that the mean residence time varies at piedmont outlets. We propose that the internal dynamics of alluvial rivers can generate strong autogenic fluctuations in sediment residence times at their outlets, over timescales of hundreds of thousands of years. As recycling should increase during the orogenic cycle, it is expected that residence-time dependent proxies integrate an increasing period of time as deposits become younger. Paradoxically, younger deposits that have a higher stratigraphic resolution may lose temporal resolution in their paleo-environmental proxies because these proxies integrate older grains, potentially masking recent climatic variations. One way to evaluate the effect of recycled old grains may be to divide each sample into grains or aliquots and to measure the proxy in each aliquot when possible.

5 Conclusion

We show simulations of mountain-piedmont systems that have reached a macroscopic equilibrium, i.e. a mountain eroding at the same rate as it is uplifting and a piedmont acting as a by-pass for sediment exported from the mountain over long timescales. This equilibrium is however imperfect as episodic sedimentation, associated with alluvial piedmont dynamics and their coupling with mountain erosion dynamics, suggests that sediment can be stored for Ma in the piedmont before being exported. As a result, the residence time of grains in the piedmont is distributed over a very large range, and a range that varies with time. Grains with long residence times significantly increase the mean residence time of a population of grains, such that the mean residence time of grains in a sample can be orders of magnitude larger than 95% of the grains. Consequently, paleo-environmental proxies of mean residence times recorded in onshore or offshore basins may produce a maximum value well above that of the majority of grains in a sample. Variation in these proxies may be partly explained by stochastic variability in the processes that recycle old grains.

Acknowledgments

This paper is a contribution to LMI COPEDIM funded by IRD. L.G. is funded by the COLORS project. R.H. is funded by the Research Center for Integrated Disaster Risk Management (CIGIDEN) ANID/FONDAP/15110017. The funding sources had no involvement in the preparation of this manuscript. We thank Frédéric Christophoul for discussions. Valerie Chavagnac is thanked for useful feedback, although we are alone responsible for any error or misconception. We thank Fritz Schlunegger and an anonymous reviewer for their constructive reviews.

Color figures: Color should be used for any figures in print.

Competing interests statement: The authors have no competing interests to declare.

Appendix A CIDRE Model and parameters values

A.1 Erosion and sedimentation

Starting from an initial topography, the modification of the topography proceeds with successive time-steps. During a time-step, precipitation falls on the grid at a rate P [LT^{-1}] and a multiple flow algorithm propagates the water flux Q [L^{3}T^{-1}] towards all downstream cells in proportion to the slope in each direction. Then the elevation z (river bed or hillslope surface) changes on each cell (size dx) according to the balance between erosion ϵ [LT^{-1}] and deposition D [LT^{-1}]. The erosion is different for sediment and for bedrock and ϵ is the sum of two values, one corresponding to gravitational processes without involving the runoff, usually dominating on the hillslopes, and another one associated with water discharge, typically dominating in rivers. Water flowing in one direction is also able to detach material from the cells located perpendicular to this direction to simulate river bank erosion. This erosion generates a lateral (bank) sediment discharge q_{sl} [L^{2}T^{-1}] towards the cell where the water is flowing. Finally, elevation also changes by adding an uplift U [LT^{-1}] (subsidence if negative).

The rate of elevation change on a cell is determined by the following mass balance equation (e.g. *Davy and Lague*, 2009; *Carretier et al.*, 2016; *Shobe et al.*, 2017):

$$\frac{\partial z}{\partial t} = -\epsilon_r - \epsilon_h + D_r + D_h - \frac{dq_{sl}}{dx} + U \qquad (1)$$

where the subscript "r" ("river") denotes rates associated with flowing water and "h" ("hillslope") denotes rates that depends only on the topographic gradient or slope S. Then we define a constitutive law for each of these components: (*Carretier et al.*, 2016)

$$\epsilon_r = Kq^m S^n \text{ for river processes} \qquad (2)$$

$$\epsilon_h = \kappa S \text{ for hillslope processes} \qquad (3)$$

where K [L^{1-2m}T^{m-1}], κ [LT^{-1}] are erodibility parameters, m and n are lithology-dependent (different for bedrock or sediment) erosion parameters, S is the slope, q [L^{3}T^{-1}] is the water discharge per stream unit width, and

$$D_r = \frac{q_{sr}}{\zeta q} \text{ for river processes} \quad (4)$$

$$D_h = \frac{q_{sh}}{\frac{dx}{1-(S/S_c)^2}} \text{ for hillslope processes} \quad (5)$$

where q_{sr} and q_{sh} are the incoming river and hillslope sediment fluxes (total $q_s = q_{sr} + q_{sh}$) per unit width [$\mathrm{L}^2\mathrm{T}^{-1}$], ζ is a river transport length parameter [T L^{-1}] and S_c is a slope threshold. These fluxes are the sum of sediment fluxes leaving upstream neighbour cells while the deposition rates on a cell are a fraction of the incoming sediment.

Concerning the river processes, ϵ_r is known as the stream power law and derives from the assumption that ϵ_r is proportional to a power law of the shear stress or to the unit stream power applied by the flowing water on the river bed (e.g. *Whipple et al.*, 2000; *Lague*, 2014)

$$\epsilon_r \propto \tau^a \quad (6)$$

ϵ_r is proportional to the river bottom shear stress τ if $a = 1$ and to the unit stream power if $a = 1.5$. ϵ_r can also depend on a critical shear stress for detachment but we neglect it here. Assuming steady, uniform flow in a wide channel, and using the Manning equation for the resistance to water flow by river bed friction (e.g. *Tucker*, 2004) then

$$\epsilon_r \propto q^{0.7a} S^{0.7a} \quad (7)$$

or

$$\epsilon_r \propto (\frac{Q}{w})^{0.7a} S^{0.7a} \quad (8)$$

where w is the river width and Q the volumetric water discharge. Considering classical river width-discharge relationship (*Leopold and Maddock*, 1953) neglecting the effect of slope (*Finnegan et al.*, 2005)

$$w \propto Q^{0.5} \quad (9)$$

then

$$\epsilon_r \quad \propto \quad Q^{0.7a-0.5} S^{0.7a} \tag{10}$$

dividing Q by the pixel width dx leads to the form of Equation 2 where $m = 0.7a - 0.5$ and $n = 0.7a$. With a between 1 and 1.5, m varies between 0.2 and 0.5, whereas n varies between 0.7 and 1. In the simulations presented in this paper, we use $m = 0.3$ or $m = 0.5$. Considering the cumulative contribution of the full discharge distribution and a non zero critical shear stress to parametrize ϵ_r leads to the same form of Equation 2 but with different values of m and n (e.g. *Lague*, 2014). In particular, n is thought to be larger than 1 in mountain rivers, what motivated our choice to take $n = 1.3$ for bedrock. Alternatively, we could have set a non zero critical shear stress and have imposed a distribution of precipitation events as input parameters in our simulations, as done for example by *Tucker* (2004). Nevertheless, in that case, it is more difficult to control the numerical stability of the model in the piedmont area. To ensure that the autogenic variations of rivers is physical and not numerical, we preferred to use the time-averaged form of the stream power law in Equation 2.

The deposition rate D_r is a fraction of the incoming sediment flux and this fraction (ζq) has the dimension of the inverse of a length. We call this length a transport length because it has the physical meaning of a characteristic distance over which a volume of detached material will transit downstream before being deposited. In particular, when the local q is large, little sediment eroded from upstream will deposit on the cell. The transport length depends on ζ, proportional to the inverse of a settling velocity of sediment in water (e.g. *Davy and Lague*, 2009; *Lajeunesse et al.*, 2013). In instantaneous river models, ζ should be fixed by the grain size of sediment. In landscape evolution models, where the water discharge q averages the periods with and without transport, ζ is an "apparent" parameter that can take a large range of values in real situations depending on climate variability (*Guerit et al.*, 2019).

Note that in this erosion-deposition model, the transport capacity q_t is implicit and emerges from Equations 1 and 4 (see discussion in *Davy and Lague*, 2009). Considering only the river processes without lateral erosion

$$\frac{\partial z}{\partial t} \quad = \quad \frac{q_s}{\zeta q} - \epsilon_r + U \tag{11}$$

or

$$\frac{\partial z}{\partial t} = \frac{q_s - q_t}{\zeta q} + U \tag{12}$$

Where the transport capacity is defined as

$$q_t = \zeta q \epsilon_r \tag{13}$$

Consequently, q_t scales with $q^{1.2}$ if $a = 1$ and with $q^{1.5}$ if $a = 1.5$. This scaling is consistent with many coarse to fine sediment transport formulae. For example, $q_t \propto q^{1.2} \propto \tau^{1.8}$ that is close to the scaling $q_t \propto \tau^{1.6}$ in the Meyer-Peter and Muller formulae for gravel (*Wong and Parker*, 2006).

Concerning the hillslopes processes, the philosophy is the same, except that the detachment rate ϵ_r and the deposition rate D_r depend only on the slope. The linear slope dependence of ϵ_r describes diffusion processes. D_r depends on a specified critical slope S_c: when the slope is close to S_c, the deposition rate D_r decreases rapidly, simulating, on average, the onset of shallow landslides. The transport length associated with gravitational processes ($\frac{dx}{1-(S/S_c)^2}$) is inversely proportional to the probability of depositing sediment on the cell. This erosion-deposition formulation leads to similar solutions as the critical slope-dependent hillslope model studied for example by *Roering et al.* (1999) (*Carretier et al.*, 2016).

Flowing water in each direction can erode lateral cells perpendicular to that direction. Little is known about the law that describes the widening rate of vallies therefore establishing a lateral erosion law suitable for landscape evolution models, which average processes over millennia, is a challenge (*Langston and Tucker*, 2018; *Langston and Temme*, 2019). Here, the lateral sediment flux per unit length q_{sl} [L^2T^{-1}] eroded from a lateral cell is simply defined as a fraction of the river sediment flux q_{sr} [L^2T^{-1}] in the considered direction (e.g. *Murray and Paola*, 1997; *Nicholas and Quine*, 2007), assuming that lateral mobility of channels, and thus lateral erosion, increases with the flux of river sediment (*Bufe et al.*, 2016, 2019):

$$q_{sl} = \alpha\, q_{sr} \tag{14}$$

where α is a bank erodibility coefficient. α is specified for loose material (sediment) and is implicitly determined for bedrock layers, such that the ratio of lateral erodabilities is equal to the ratio of fluvial erodabilities ($\alpha_{loose}/\alpha_{bedrock} = K_{loose}/K_{bedrock}$, with K from Equation 2). If sediment covers the bedrock of a lateral cell, α is weighted by its respective thickness above the target cell.

Finally, the sediment leaving a cell is spread in the same way as water, i.e. proportionally to the downstream slopes. This procedure starts from the most elevated cell and ends with the lowest cell and is repeated in the next time-steps until the end of the specified model time (m.y. in our case).

A.2 Grain tracers

At the end of a time-step, once the grids of erosion and deposition rates are known, grain tracers are moved. Grains are spheres with a radius r. In the following simulations, thousands of grains are set randomly at the surface of the steady-state topography, with grain sizes ranging from 1 mm up to 10 cm. We therefore consider the coarse sand and gravel fractions of the sedimentary load, mostly transported as bedload by rivers. Each grain is independent of the others. At each time-step, a grain located in a given cell moves if its depth is shallower than the eroded thickness calculated over the time-step on that cell. To account for preferential erosion and transport according to the size of a grain, the probability of leaving the cell is inversely proportional to the grain size (*Carretier et al.*, 2016). Grains entering a cell have a probability to be deposited set by the ratio between the local deposition flux and the incoming sediment flux. Their probability to go in one of the downstream directions (i.e. to cross a cell) is simply the ratio of the local slope and the sum of the downstream slopes. During a time-step grains are moved until they are deposited on a cell or leave the model. When a grain crosses the line separating the mountain from the piedmont, its clock is set to zero and then increments at each time-step until it exits the model domain at the lowest border.

A.3 Parameter values for the reference simulation

In the following simulations, the uplifted domain grid is 60x40 km^2 (300x200 cells of size 200 m), and the piedmont domain is also 60x40 km^2 in the reference experiment (Fig. 1) but varies in other ones. For the bedrock, we use $K = 3.10^{-4}$ m$^{-0.2}$ yr$^{-0.4}$, $m = 0.6$, $n = 1.3$ and $\kappa = 10^{-4}$ m yr^{-1}. These parameters are motivated by evidences that $n > 1$ (*Harel et al.*, 2016; *Clubb* *et al.*, 2016; *Deal et al.*, 2017) and generate a final realistic maximum relief of $\sim$1700 m. For the sediment, we use $K = 6.10^{-3}$ m$^{0.4}$ yr$^{-0.7}$, $m = 0.3$, $n = 1$ and $\kappa = 2.10^{-4}$ m yr^{-1}. With these values, for a given slope and discharge, erosion of sediment is larger than bedrock. The transport length parameter ζ is set to 0.1 yr m^{-1}, and corresponds to a low value for natural systems (median at 17 yr/m *Guerit et al.*, 2019). It is difficult to link ζ with physical properties of sediment because ζ changes according to the variability of transport periods, but low values seem to correspond to temperate perennial rivers (*Guerit et al.*, 2019). The lateral erosion parameter α is set as 5.10^{-4}. Finally, the critical slope is S_c =tan(40^o). The northern side of the model is closed (i.e. no water nor sediment can leave the model through this side) while the south boundary is open and fixed to $z = 0$ m. Periodic boundary conditions are imposed on the two other sides meaning that material leaving on one side is reinjected at the other.

U is fixed to 10^{-3} m yr^{-1} and there is no subsidence in the piedmont. We discuss subsidence extensively in the Discussion. Although we want to design the simplest simulations, we incorporate a precipitation gradient with elevation that characterises most mountain-foreland systems and may influence the sediment residence time in the piedmont. Starting from a precipitation rate of 1 m yr^{-1} at baselevel, P varies dynamically with elevation z according to a specified relationship similar to a Gaussian curve that reaches a maximum of 1.7 m yr^{-1} at 1300 m, a peak elevation usually found in the Himalaya or Andes (*Bookhagen and Burbank*, 2006; *Bookhagen and Strecker*, 2008; *Colberg and Anders*, 2014):

$$P(z) = 1. + 0.7e^{\frac{(z-1300)^2}{2.1300^2}} \tag{15}$$

References

Allen, P. A., J. J. Armitage, A. Carter, R. A. Duller, N. A. Michael, H. D. Sinclair, A. L. Whitchurch, and A. C. Whittaker (2013), The Qs problem: Sediment volumetric balance of proximal foreland basin systems, *Sedimentology*, *60*(1, SI), 102–130, doi:10.1111/sed.12015.

Allison, M., S. Kuehl, T. Martin, and A. Hassan (1998), Importance of floodplain sedimentation for river sediment budgets and terrigenous input to the oceans: Insights from the brahmaputra-jamuna river, *Geology*, *26*(2), 175–178.

Armitage, J., T. Jones, R. Duller, A. Whittaker, and P. Allen (2013), Temporal buffering of climate-driven sediment flux cycles by transient catchment response, *Earth and Planetary Science Letters*, *369*, 200–210.

Babault, J., S. Bonnet, A. Crave, and J. van den Driessche (2005), Influence of piedmont sedimentation on erosion dynamics of an uplifting landscape: An experimental approach, *Geology*, *33(4)*, 301–304.

Bekaddour, T., F. Schlunegger, H. Vogel, R. Delunel, K. Norton, N. Akçara, and P. Kubik (2014), Paleo erosion rates and climate shifts recorded by Quaternary cut-and-fill sequences in the Pisco valley, central Peru, *Earth Planet. Sci. Lett.*, *390*, 103–115.

Bernal, C., F. Christophoul, J. Darrozes, J.-C. Soula, P. Baby, and J. Burgos (2011), Late Glacial and Holocene avulsions of the Rio Pastaza Megafan (Ecuador-Peru): frequency and controlling factors, *Int. Journal Of Earth Sciences*, *100*(7), 1759–1782, doi:10.1007/s00531-010-0555-9.

Blöthe, J. H., and O. Korup (2013), Millennial lag times in the himalayan sediment routing system, *Earth and Planetary Science Letters*, *382*, 38–46.

Bonnet, S., T. Reimann, J. Wallinga, D. Lague, P. Davy, and A. Lacoste (2019), Landscape dynamics revealed by luminescence signals of feldspars from fluvial terraces, *Scientifc Reports*, *9*, doi:10.1038/s41598-019-44533-4.

Bookhagen, B., and D. W. Burbank (2006), Topography, relief, and trmm-derived rainfall variations along the himalaya, *Geophysical Research Letters*, *33*(8).

Bookhagen, B., and M. R. Strecker (2008), Orographic barriers, high-resolution TRMM rainfall, and relief variations along the eastern Andes, *Geophys. Res. Lett.*, *35*, L06,403, doi:10.1029/2007GL032011.

Bradley, D. N., and G. E. Tucker (2013), The storage time, age, and erosion hazard of laterally accreted sediment on the floodplain of a simulated meandering river, *J. Geophys. Res. Earth Surface*, *118*(3), 1308–1319, doi:10.1002/jgrf.20083.

Bufe, A., C. Paola, and D. W. Burbank (2016), Fluvial bevelling of topography controlled by lateral channel mobility and uplift rate, *Nature Geoscience*, *9*(9), 706.

Bufe, A., J. M. Turowski, D. W. Burbank, C. Paola, A. D. Wickert, and S. Tofelde (2019), Controls on the lateral channel-migration rate of braided channel systems in coarse non-cohesive sediment, *Earth Surf. Proc. Land.*, *44*(14), 2823–2836, doi:10.1002/esp.4710.

Burbank, D. (1992), Causes of recent Himalayan uplift deduced from deposited patterns in the Ganges basin, *Nature*, *357*(6380), 680–683, doi:10.1038/357680a0.

Carretier, S., and F. Lucazeau (2005), How does alluvial sedimentation at range fronts modify the erosional dynamics of mountain catchments?, *Basin Res.*, *17*, 361–381, doi:10.1111/j.1365-2117.2005.00270.x.

Carretier, S., P. Martinod, M. Reich, and Y. Goddéris (2016), Modelling sediment clasts transport during landscape evolution, *Earth Surf. Dynam.*, *4*, 237–251, doi:10.5194/esurf-4-237-2016.

Carretier, S., Y. Godderis, J. Martinez, M. Reich, and P. Martinod (2018), Colluvial deposits as a possible weathering reservoir in uplifting mountains, *Earth Surface Dynamics*, *6*(1), 217–237, doi:10.5194/esurf-6-217-2018.

Carretier, S., V. Regard, L. Leanni, and M. Farias (2019), Long-term dispersion of river gravel in a canyon in the Atacama Desert, Central Andes, deduced from their 10Be concentrations, *Scientific Reports*, *9*, 17,763, doi: https://doi.org/10.1038/s41598-019-53806-x.

Cederbom, C., H. Sinclair, F. Schlunegger, and M. Rahn (2004), Climate-induced rebound and exhumation of the European Alps, *Geology*, *32*(8), 709–712, doi:10.1130/G20491.1.

Chabaux, F., M. Granet, E. Pelt, C. France-Lanord, and V. Galy (2006), 238U-234U-230Th disequilibria and timescale of sedimentary transfers in rivers: clues from the Gangetic plain rivers, *Journal of Geochemical Exploration*, *88*, 373–375.

Clarke, L., T. Quine, and A. Nicholas (2010), An experimental investigation of autogenic behaviour during alluvial fan evolution, *Geomorphology*, *115*, 278–285.

Clift, P. (2006), Controls on the erosion of Cenozoic Asia and the flux of clastic sediment to the ocean, *Earth Planet. Sci. Lett.*, *241*(3-4), 571–580, doi:10.1016/j.epsl.2005.11.028.

Clift, P. D., and L. Giosan (2014), Sediment fluxes and buffering in the post-glacial Indus Basin, *Basin Res.*, *26*(3), 369–386, doi:10.1111/bre.12038.

Clift, P. D., and A. A. G. Webb (2018), A history of the asian monsoon and its interactions with solid earth tectonics in cenozoic south asia, *Geological Society, London, Special Publications*, *483*, SP483–1.

Clift, P. D., K. V. Hodges, D. Heslop, R. Hannigan, H. Van Long, and G. Calves (2008), Correlation of Himalayan exhumation rates and Asian monsoon intensity, *Nature GeoSciences*, *1*(12), 875–880, doi:10.1038/ngeo351.

Clubb, F. J., S. M. Mudd, M. Attal, D. T. Milodowski, and S. W. D. Grieve (2016), The relationship between drainage density, erosion rate, and hilltop curvature: Implications for sediment transport processes, *J. Geophys. Res. Earth Surface*, *121*(10), doi:10.1002/2015JF003747.

Colberg, J. S., and A. M. Anders (2014), Numerical modeling of spatially-variable precipitation and passive margin escarpment evolution, *Geomorphology*, *207*, 203–212, doi:10.1016/j.geomorph.2013.11.006.

Davy, P., and D. Lague (2009), The erosion / transport equation of landscape evolution models revisited, *J. Geophys. Res.*, *114*, doi:10.1029/2008JF001146.

Deal, E., A.-C. Favre, and J. Braun (2017), Rainfall variability in the himalayan orogen and its relevance to erosion processes, *Water Resources Research*, *53*(5), 4004–4021.

DeCelles, P. G., M. B. Gray, K. D. Ridgway, R. B. Cole, D. A. Pivnik, N. Pequera, and P. Srivastava (1991), Controls on synorogenic alluvial-fan architecture, Beartooth Conglomerate (Palaeocene), Wyoming and Montana, *Sedimentology*, *38*(4), 567–590.

Di Giulio, A., A. Ceriani, E. Ghia, and F. Zucca (2003), Composition of modern stream sands derived from sedimentary source rocks in a temperate climate (northern apennines, italy), *Sedimentary Geology*, *158*(1-2), 145–161.

Dingle, E., H. Sinclair, J. Venditti, M. Attal, T. Kinnaird, M. Creed, L. Quick, J. Nittrouer, and D. Gautam (2020), Sediment dynamics across gravel-sand transitions: Implications for river stability and floodplain recycling, *Geology*, (48), , doi:https://doi.org/10.1130/G46909.1.

Dosseto, A., B. Bourdon, J. Gaillardet, L. Maurice-Bourgoin, and C. Allègre (2006), Weathering and transport of sediments in the Bolivian Andes: Time constraints from uranium-series isotopes, *Earth Planet. Sci. Lett.*, *248*, 759–771.

Duller, R. A., A. C. Whittaker, J. J. Fedele, A. L. Whitchurch, J. Springett, R. Smithells, S. Fordyce, and P. A. Allen (2010), From grain size to tectonics, *J. Geophys. Res. Earth Surface*, *115*, doi:10.1029/2009JF001495.

Einstein, H.A. (1937), Bed load transport as a probability problem, Ph.D. thesis, ETH Zurich.

Fedele, J. J., and C. Paola (2007), Similarity solutions for fluvial sediment fining by selective deposition, *J. Geophys. Res. Earth Surface*, *112*(F2), F02,038, doi:10.1029/2005JF000409.

Field, J. (2001), Channel avulsion on alluvial fans in southern Arizona, *Geomorphology*, *37*(1), 93–104.

Finnegan, N., G. Roe, D. R. Montgomery, and B. hallet (2005), Controls on the channel width of rivers: Implications for modeling fluvial incision of bedrock, *Geology*, *33*, 229–232, doi:10.1130/G21171.1.

Flood, Y. S., and G. J. Hampson (2014), Facies and architectural analysis to interpret avulsion style and variability: Upper cretaceous blackhawk formation, wasatch plateau, central utah, usa, *Journal of Sedimentary Research*, *84*(9), 743–762.

Foreman, B. Z., and K. M. Straub (2017), Autogenic geomorphic processes determine the resolution and fidelity of terrestrial paleoclimate records, *Science Advances*, *3*(9), doi:10.1126/sciadv.1700683.

Gabet, E., and S. Mudd (2009), A theoretical model coupling chemical weathering rates with denudation rates, *Geology*, *37*, 151–154.

Ganti, V., C. von Hagke, D. Scherler, M. P. Lamb, W. W. Fischer, and J.-P. Avouac (2016), Time scale bias in erosion rates of glaciated landscapes, *Science Advances*, *2*(10), doi:10.1126/sciadv.1600204.

Garzanti, E., G. Vezzoli, S. Andò, J. Lavé, M. Attal, C. France-Lanord, and P. DeCelles (2007), Quantifying sand provenance and erosion (marsyandi river, nepal himalaya), *Earth and Planetary Science Letters*, *258*(3-4), 500–515.

Giosan, L., P. D. Clift, M. G. Macklin, D. Q. Fuller, S. Constantinescu, J. A. Durcan, T. Stevens, G. A. T. Duller, A. R. Tabrez, K. Gangal, R. Adhikari, A. Alizai, F. Filip, S. VanLaningham, and J. P. M. Syvitski (2012), Fluvial landscapes of the Harappan civilization, *PNAS*, *109*(26), E1688–E1694, doi:10.1073/pnas.1112743109.

Goodbred, S., and S. Kuehl (2003), The production, transport, and accumulation of sediment: a cross-section of recent developments with an emphasis on climate effects, *Sedimentary Geology*, *162*(1-2), 1–3, doi:10.1016/S0037-0738(03)00215-X.

Granet, M., F. Chabaux, P. Stille, C. France-Lanord, and E. Pelt (2007), Time-scales of sedimentary transfer and weathering processes from u-series nuclides: clues from the himalayan rivers, *Earth and Planetary Science Letters*, *261*(3-4), 389–406.

Guerit, L., L. Barrier, M. Jolivet, B. Fu, and F. Métivier (2016), Denudation intensity and control in the Chinese Tian Shan: new constraints from mass balance on catchment-alluvial fan systems, *Earth Surface Processes and Landforms*, *41*(8), 1088–1106.

Guerit, L., X.-P. Yuan, S. Carretier, S. Bonnet, S. Rohais, J. Braun, and D. Rouby (2019), Fluvial landscape evolution controlled by the sediment deposition coefficient: Estimation from experimental and natural landscapes, *Geology*, *47*(9), 853–856, doi:10.1130/G46356.1.

Hajek, E., P. Heller, and E. Schur (2012), Field test of autogenic control on alluvial stratigraphy (ferris formation, upper cretaceous–paleogene, wyoming), *Bulletin*, *124*(11-12), 1898–1912.

Hajek, E. A., P. L. Heller, and B. A. Sheets (2010), Significance of channel-belt clustering in alluvial basins, *Geology*, *38*(6), 535–538.

Hancock, G. S., and R. S. Anderson (2002), Numerical modeling of fluvial strath-terrace formation in response to oscillating climate, *Geol. Soc. Am. Bull.*, *114*, 1131–1142.

Harel, M.-A., S. Mudd, and M. Attal (2016), Global analysis of the stream power law parameters based on worldwide 10be denudation rates, *Geomorphology*, *268*, 184–196.

Harries, R. M., L. A. Kirstein, A. C. Whittaker, M. Attal, and M. I. (2019), Impact of recycling and lateral sediment input on grain size fining trends?Implications for reconstructing tectonic and climate forcings in ancient sedimentary systems, *Basin Res.*, pp. 1–26, doi:10.1111/bre.12349.

Hoffmann, T. (2015), Sediment residence time and connectivity in non-equilibrium and transient geomorphic systems, *Earth-Science Reviews*, *150*, 609–627, doi:10.1016/j.earscirev.2015.07.008.

Hofmann, M. H., A. Wroblewski, and R. Boyd (2011), Mechanisms controlling the clustering of fluvial channels and the compensational stacking of cluster belts, *Journal of Sedimentary Research*, *81*(9), 670–685.

Hovius, N., C. P. Stark, C. Hao-Tsu, and L. Jiun-Chuan (2000), Supply and removal of sediment in a landslide-dominated mountain belt: Central Range, Taiwan, *J. Geol*, *108*, 73–89.

Hu, D., P. Boening, C. M. Koehler, S. Hillier, N. Pressling, S. Wan, H. J. Brumsack, and P. D. Clift (2012), Deep sea records of the continental weathering and erosion response to East Asian monsoon intensification since 14 ka in the South China Sea, *Chem. Geol.*, *326*, 1–18, doi:10.1016/j.chemgeo.2012.07.024.

Humphrey, N., and P. L. Heller (1995), Natural oscillations in coupled geomorphic systems: an alternative origin for cyclic sedimentation, *Geology*, *23*, 499–502.

Jolivet, M., L. Barrier, S. Dominguez, L. Guerit, G. Heilbronn, and B. Fu (2014), Unbalanced sediment budgets in the catchment - alluvial fan system of the Kuitun River (northern Tian Shan, China): Implications for the erosion and uplift rate estimates in mountain ranges, *Geomorphology*, *214*, 168 – 182.

Jonell, T. N., L. A. Owen, A. Carter, J.-L. Schwenniger, and P. D. Clift (2018), Quantifying episodic erosion and transient storage on the western margin of the Tibetan Plateau, upper Indus River, *Quaternary Research*, *89*(1, SI), 281–306, doi:10.1017/qua.2017.92.

Kim, W., and D. J. Jerolmack (2008), The pulse of calm fan deltas, *The Journal of Geology*, *116*(4), 315–330, doi:10.1086/588830.

Kim, W., C. Paola, J. B. Swenson, and V. R. Voller (2006), Shoreline response to autogenic processes of sediment storage and release in the fluvial system, *Journal of Geophysical Research: Earth Surface*, *111*(F4).

Lague, D. (2014), The stream power river incision model: evidence, theory and beyond, *Earth Surf. Proc. Land.*, *39*(1), 38–61, doi:10.1002/esp.3462.

Lajeunesse, E., O. Devauchelle, M. Houssais, and G. Seizilles (2013), Tracer dispersion in bedload transport, *Advances in GeoSciences*, *37*, doi: 10.5194/adgeo-37-1-2013.

Lang, K. A., T. A. Ehlers, P. J. J. Kamp, and U. Ring (2018), Sediment storage in the Southern Alps of New Zealand: New observations from tracer thermochronology, *Earth Planet. Sci. Lett.*, *493*, 140–149, doi: 10.1016/j.epsl.2018.04.016.

Langston, A. L., and A. J. A. M. Temme (2019), Bedrock erosion and changes in bed sediment lithology in response to an extreme flood event: The 2013 Colorado Front Range flood, *Geomorphology*, *328*, 1–14, doi: 10.1016/j.geomorph.2018.11.015.

Langston, A. L., and G. E. Tucker (2018), Developing and exploring a theory for the lateral erosion of bedrock channels for use in landscape evolution models, *Earth Surface Dynamics*, *6*(1), 1–27, doi:10.5194/esurf-6-1-2018.

Lauer, J. W., and J. Willenbring (2010), Steady state reach-scale theory for radioactive tracer concentration in a simple channel/floodplain system, *J. Geophys. Res. Earth Surface*, *115*, doi:10.1029/2009JF001480.

Leopold, L. B., and T. J. Maddock (1953), The hydrolic geometry of stream channels and some physiographic implications, *U. S. Geol. Survey. Professional Paper*, *252*, 57.

Li, C., S. Yang, J.-x. Zhao, A. Dosseto, L. Bi, and T. R. Clark (2016a), The time scale of river sediment source-to-sink processes in East Asia, *Chemical Geology*, *446*(SI), 138–146, doi:10.1016/j.chemgeo.2016,06.012.

Li, Q., L. Yu, and K. M. Straub (2016b), Storage thresholds for relative sea-level signals in the stratigraphic record, *Geology*, *44*(3), 179–182, doi: 10.1130/G37484.1.

MacKenzie, L. G., and B. C. Eaton (2017), Large grains matter: contrasting bed stability and morphodynamics during two nearly identical experiments, *Earth Surf. Proc. Land.*, *42*(8), 1287–1295, doi:10.1002/esp.4122.

Malatesta, L., J.-P. Avouac, N. Brown, S. Breitenbach, J. Pan, M.-L. Chevalier, E. Rhodes, D. Saint-Carlier, W. Zhang, J. Charreau, J. Lavé, and P.-H. Blard (2018), Lag and mixing during sediment transfer across the tian shan piedmont caused by climate-driven aggradation–incision cycles, *Basin Research*, (30(4)), 613–635.

Martin, A. N., A. Dosseto, J.-H. May, J. D. Jansen, L. P. Kinsley, and A. R. Chivas (2019), Sediment residence times in catchments draining to the gulf of carpentaria, northern australia, inferred by uranium comminution dating, *Geochimica et Cosmochimica Acta*, *244*, 264–291.

Metivier, F., Y. Gaudemer, P. Tapponnier, and M. Klein (1999), Mass accumulation rates in Asia during the Cenozoic, *Geophys J Int.*, *137(2)*, 280–318, doi:10.1046/j.1365-246X.1999.00802.x.

Mondal, M. E. A., H. Wani, and B. Mondal (2012), Geochemical signature of provenance, tectonics and chemical weathering in the Quaternary flood plain sediments of the Hindon River, Gangetic plain, India, *Tectonophysics*, *566*, 87–94, doi:10.1016/j.tecto.2012.07.001.

Mudd, S., and K. Yoo (2010), Reservoir theory for studying the geochemical evolution of soils, *J. Geophys. Res.*, *115*, F03,030, doi:10.1029/2009JF001591.

Murray, A. B., and C. Paola (1997), Properties of a cellular braided-stream model, *Earth Surf. Proc. Land.*, *22*, 1001–1025.

Nicholas, A., and T. Quine (2007), Modeling alluvial landform change in the absence of external environmental forcing, *Geology*, *35*, 527–530, doi:10.1130/G23377A.1.

Paola, C., K. Straub, D. Mohrig, and L. Reinhardt (2009), The "unreasonable effectiveness" of stratigraphic and geomorphic experiments, *Earth-Science Reviews*, *97*(1-4), 1–43, doi:10.1016/j.earscirev.2009.05.003.

Parker, G., Member, ASCE, C. Poala, K. X. Whipple, and D. Mohrig (1998), Alluvial fans formed by channelized fluvial and sheet flow. I: Theory, *Journal of Hydraulic Engineering*, *124(10)*, 985–995.

Powell, E. J., W. Kim, and T. Muto (2012), Varying discharge controls on timescales of autogenic storage and release processes in fluvio-deltaic environments: Tank experiments, *Journal of Geophysical Research*, *117*.

Quick, L., H. Sinclair, M. Attal, and V. Singh (2019), Conglomerate recycling in the Himalayan foreland basin: Implications for grain size and provenance, *Geol. Soc. Am. Bull.*, *in press*, doi:https://doi.org/10.1130/B35334.1.

Reitz, M., and D. Jerolmack (2012), Experimental alluvial fan evolution: Channel dynamics, slope controls, and shoreline growth, *Journal of Geophysical Research*, *117*.

Reitz, M. D., D. J. Jerolmack, and J. B. Swenson (2010), Flooding and flow path selection on alluvial fans and deltas, *GRL*, *37*, doi:10.1029/2009GL041985.

Riquelme, R., M. Tapia, E. Campos, C. Mpodozis, S. Carretier, R. González, S. Munoz, A. Fernández-Mort, C. Sanchez, and C. Marquardt (2018), Supergene and exotic cu mineralization occur during periods of landscape stability in the centinela mining district, atacama desert, *Basin Research*, *30*(3), 395–425.

Roering, J. J., J. W. Kirchner, and W. E. Dietrich (1999), Evidence for nonlinear, diffusive sediment transport on hillslopes and implications for landscape morphology, *Wat. Resour. Res.*, *35*, 853–870.

Rohais, S., S. Bonnet, and R. Eschard (2012), Sedimentary record of tectonic and climatic erosional perturbations in an experimental coupled catchment-fan system, *Basin Res.*, *24*(2), 198–212, doi:10.1111/j.1365-2117.2011.00520.x.

Schumm, S., M. Mosley, and W. Weaver (1987), *Experimental fluvial geomorphology*, John Wiley and Sons Inc., New York, NY.

Shobe, C. M., G. E. Tucker, and K. R. Barnhart (2017), The SPACE 1.0 model: a Landlab component for 2-D calculation of sediment transport, bedrock erosion, and landscape evolution, *Geoscientific Model Development*, *10*(12), 4577–4604, doi:10.5194/gmd-10-4577-2017.

Sinclair, H. D., F. M. Stuart, S. M. Mudd, L. McCann, and Z. Tao (2019), Detrital cosmogenic Ne-21 records decoupling of source-to-sink signals by sediment storage and recycling in Miocene to present rivers of the Great Plains, Nebraska, USA, *Geology*, *47*(1), 3–6, doi:10.1130/G45391.1.

Tucker, G. (2004), Drainage basin sensitivity to tectonic and climatic forcing: Implications of a stochastic model for the role of entrainment and erosion thresholds, *Earth Surf. Proc. Land.*, *29*, 185–205, doi:10.1002/esp.1020.

Tucker, G., and P. van der Beek (2013), A model for post-orogenic development of a mountain range and its foreland, *Basin Res.*, *24*, 241–259, doi: 10.1111/j.1365-2117.2012.00559.x.

Van De Wiel, M. J., and T. J. Coulthard (2010), Self-organized criticality in river basins: Challenging sedimentary records of environmental change, *Geology*, *38*(1), 87–90, doi:10.1130/G30490.1.

van Dijk, M., G. Postma, and M. Kleinhans (2009), Autocyclic behaviour of fan deltas: an analogue experimental study, *Sedimentology*, *56*(5), 1569–1589.

Virkar, Y., and A. Clauset (2014), Power-law distributions in binned empirical data, *The Annals of Applied Statistics*, *8*(1), 89–119.

Wang, P., Y. Dua, W. Yua, T. Algeo, Q. Zhoud, Y. Xua, L. Qi, L. Yuan, and W. Pan (2019), The chemical index of alteration (CIA) as a proxy for climate change during T glacial-interglacial transitions in Earth history, *Earth Sc. Rev.*, *201*, 103,032, doi:10.1016/j.earscirev.2019.103032.

Wang, Y., K. M. Straub, and E. A. Hajek (2011), Scale-dependent compensational stacking: an estimate of autogenic time scales in channelized sedimentary deposits, *Geology*, *39*(9), 811–814.

Weltje, G. J. (2012), Quantitative models of sediment generation and provenance: State of the art and future developments, *Sedimentary Geology*, *280*(SI), 4–20, doi:10.1016/j.sedgeo.2012.03.010.

Weltje, G. J., and M. B. Brommer (2011), Sediment-budget modelling of multi-sourced basin fills: application to recent deposits of the western adriatic mud wedge (italy), *Basin Research*, *23*(3), 291–308.

Whipple, K. X., G. S. Hancock, and R. S. Anderson (2000), River incision into bedrock: Mechanics and relative efficacy of plucking, abrasion and cavitation, *Geol. Soc. Am. Bull.*, *112*, 490–503.

Whittaker, A. C., R. A. Duller, J. Springett, R. A. Smithells, A. L. Whitchurch, and P. A. Allen (2011), Decoding downstream trends in stratigraphic grain size as a function of tectonic subsidence and sediment supply, *Geol. Soc. Am. Bull.*, *123*(7-8), 1363–1382, doi:10.1130/B30351.1.

Wittmann, H., F. von Blanckenburg, L. Maurice, J.-L. Guyot, N. Filizola, and P. W. Kubik (2011), Sediment production and delivery in the amazon river basin quantified by in situ–produced cosmogenic nuclides and recent river loads, *Bulletin*, *123*(5-6), 934–950.

Wong, M., and G. Parker (2006), Reanalysis and correction of bed-load relation of Meyer-Peter and Muller using their own database, *J. of Hydraulic Engineering*, *132*(11), 1159–1168, doi:10.1061/(ASCE)0733-9429(2006)132:11(1159).

Zavala, V., S. Carretier, and S. Bonnet (2020), Influence of orographic precipitation on the topographic and erosional evolution of mountain ranges, *Basin Res.*, *in press*, doi:https://doi.org/10.1111/bre.12443.

Figure 1: Model setup illustrated with a stage of the topographic evolution that corresponds to a dynamic equilibrium between the mountain uplift and erosion in the reference simulation (the darker the blue, the larger the water discharge). The reference simulation starts with a Gaussian distribution of elevations centered to 0 m and with a deviation of 0.5 m. Then the drainage organises itself, controlled by the boundary conditions, the uplift of the mountain domain and the deposition into the piedmont domain. The east and west boundary conditions are connected, which means that water and sediment leaving the east border enters the west border and vice versa. These boundary conditions avoid "border effects". The maximum elevation is ~ 1700 m.

Figure 2: (a-) and (b-) Snapshots of the topography at two times during the period of dynamic equilibrium, showing lateral stability of the drainage network in the mountain, but varying in the piedmont (differences highlighted by the ovals). (c-) and (d-) Erosion and sediment rates for these two snapshots, demonstrate sedimentary and geomorphic features in the piedmont that are observed in all the presented simulations. Note that topographic shading creates apparent erosion rate variations in the mountain, but erosion varies only slightly around the uplift rate of 1 mm yr^{-1}. (e-) Mean stacked topographic profiles showing that dynamic variation has been reached. (f-) Time variations of a topographic cross-profile taken across the middle of the piedmont, located in (a-). Despite a macroscopic equilibrium, the piedmont is reworked over a mixing layer of 60-70 m.

Figure 3: Successive snapshots (a- to f-) of erosion and sedimentation rates and water discharge (normalised by the maximum value on the grid) illustrating the interplay between the erosional dynamics in the mountain and the depositional dynamics in the piedmont. Erosion waves are often generated during a river capture, leading to a temporary fan entrenchment at its apex that propagates into the mountain, as in panel (a-). These erosion waves are associated with higher local erosion rate and a convexity in the river profile, called a knick-point. The initiation and upstream propagation of such a knick-point is highlighted with circles and arrows in panels (a-) to (f-). The erosion waves associated with the upstream propagation of knick-points deliver a pulse of sediment which, in turn, generates lobes and splay-offs in the piedmont. This episodic deposition favours the lateral mobility of piedmont rivers, which fosters, in turn, river captures. There is thus an intimate coupling between the erosion and sedimentation dynamics in the mountain and in the alluvial apron. The topographic contour lines are every 200 m.

Figure 4: (a-) Three snapshots of topography and grain locations after their introduction at t=0 during dynamic equilibrium. 10,000 grains were randomly set at the surface of the mountain. They are then transported and when they enter the piedmont, their clock is activated. The symbol size is related to the size of the grains, which varies here between 1 and 10 cm. Note that after 1 m.y. there are still grains stored in the piedmont. (b-) Distribution of residence times (duration between entry and exit from the piedmont) taken at 2 kyr to emphasise that 95% of grains spent less than several centuries in the piedmont. Yet, the mean residence time is 18 kyr. (c-) Cumulative frequency in log-log scale to visualise the full distribution. The red symbols correspond to all grain sizes and the yellow and purple symbols correspond to selected grain sizes, with no noticeable differences. The blue symbols correspond to the same experiment but with smaller grains of 1 mm, for which the residence times are consistently smaller. In all the cases, the distribution displays a long tail, underlined by the inset segment indicators (the more gentle the segment, the longer the tail, the higher the probability to find very old grains).

Figure 5: Same as Fig. 4c (Ref - all grain sizes between 1 and 10 cm), but for different model parameters.

Figure 6: (a-) and (b-) Snapshots of grains ages (time since their entry into the piedmont) at the surface of the piedmont during dynamic equilibrium. 200,000 grains were set initially on the mountain at t=0 m.y. Part of these grains are stored in the piedmont, others leave the piedmont and are automatically replaced at their initial location in the mountain. (c-) Depth distribution of grains ages (circle size consistent with grain size) in the piedmont at 3.75 m.y. (d-) Corresponding distribution of grain ages cut at 2 m.y.

Figure 7: (a-) Time evolution of grain ages in the piedmont (one point every 10 ka). After a transient period of $\sim$0.8 m.y. for grains to cover the whole piedmont, the mean age of piedmont grains keeps on increasing because it includes grains that have been preserved from erosion for an increasing period of time. Other simulations with different parameters are also shown. (b-) and (c-) Time evolution of the mean residence time for different model parameters. In all the cases, the mean residence time shows large variations. The dashed line corresponds to the predicted turnover time in each case, i.e. the ratio between the mixing volume in the piedmont ($\sim$ 60 m times the piedmont area) and the flux of material entering the piedmont (uplift rate times mountain area). The turnover time is much larger than the residence time for most of the run because most of the exiting grains have transited quickly in rivers through the piedmont (recycled old grains are minority).

Figure 8: Same as Fig. 7 for the Ref simulation, but comparing the mean residence time calculated for grains that exited the model during the last time-step (10 yr), with the mean residence time calculated with grains that exited during the last 100 time-steps (1000 yr).

Figure 9: Different geomorphic sectors with evidence of long-tailed distributions of residence time, leading to potential recycling of old grains over the long-term ($>$ 1 kyr). All these sectors may contribute to an overestimatation of sediment residence times deduced from bulk (mean) measurements in sediment samples.

Supplementary Fig. S 1: Mean elevation, mountain erosion rate and sediment thickness in the piedmont through time. After 4 m.y. a dynamic equilibrium is reached, although there are variations in erosion rates explained by autogenic alluvial entrenchments in the piedmont and associated retreating knick-points in the mountain. After 20 m.y. of simulation, to be sure that a macroscopic dynamic equilibrium has been well established, grains are set at the surface of the mountain to trace their time spent in the piedmont.

Supplementary Fig. S 2: The same as Fig. 4 only with one grain size (1 mm) and for cases with and without lateral erosion (a -reference model and b-, respectively). The simulation without lateral erosion results in more grains leaving the piedmont quickly because the river channels are narrower (see b-) and thus grains travel faster downstream. This physical distinction explains the different cumulative frequencies (c-). Nevertheless, both distributions display a long tail, albeit shorter (or steeper trend in the log-log graph) in the case without lateral erosion. The existence of a long tail in the case that does not account for lateral erosion confirms that the lateral erosion law used in Cidre is not responsible for the long tail.

Supplementary Fig. S 3: Comparing the age of piedmont grains in the first 60 m of depth without subsidence (a- dynamic equilibrium) and with active subsidence (b-) after 2 m.y. of model time. All the parameters are the same in both experiments (parameters of the reference model), except for the simulation with subsidence: a triangular subsidence pattern is imposed in the piedmont, with a maximum subsidence rate of 0.25 mm/yr at the transition between the mountain and the piedmont, to 0 mm/yr at the downstream end of the piedmont. As grains are progressively buried at different rates along the piedmont with subsidence, only young grains ($<$ 400 kyr) are present at the alluvial fan apex, while old grains are present at the downstream end, where subsidence and burial occur at a much lower rate.

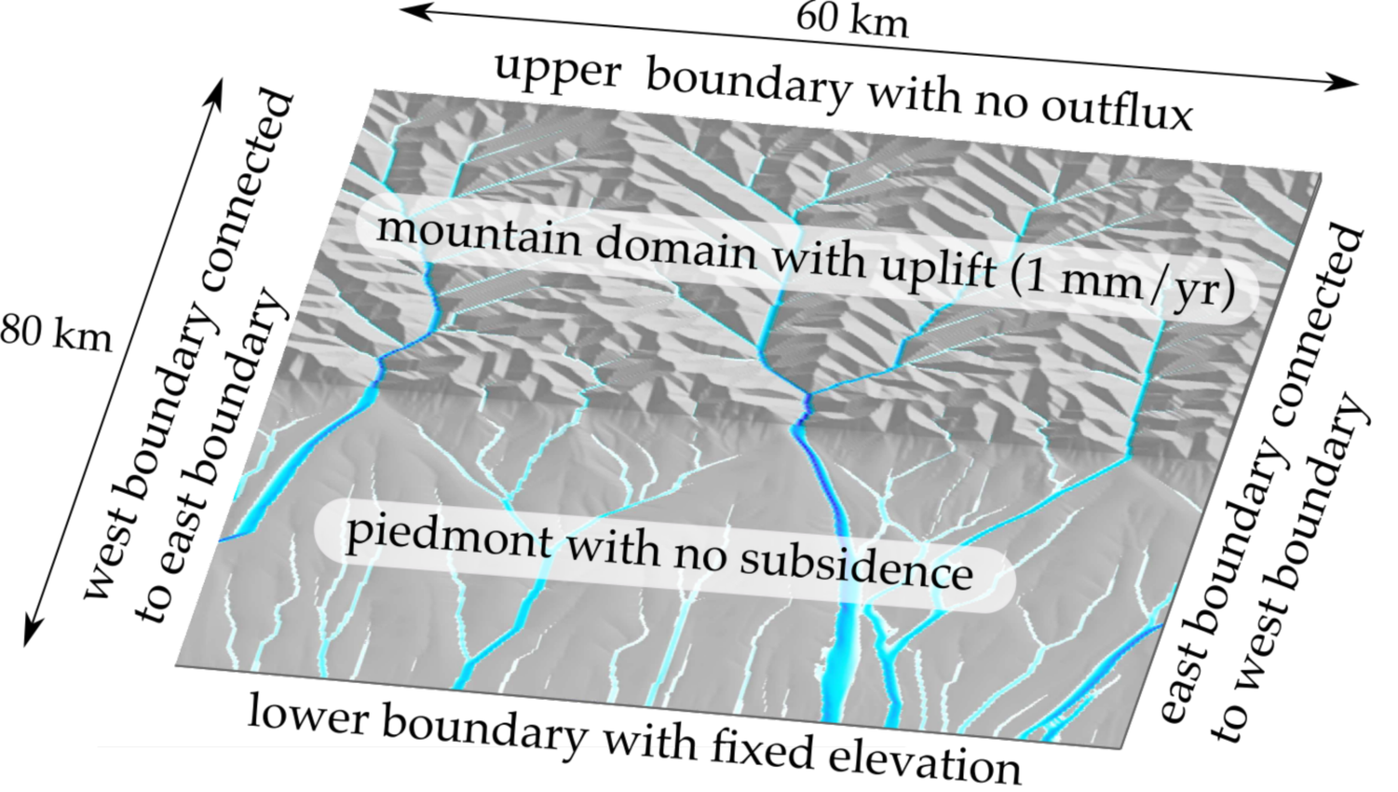

60 km
upper boundary with no outflux
80 km
west boundary connected
to east boundary
mountain domain with uplift (1 mm/yr)
piedmont with no subsidence
east boundary connected
to west boundary
lower boundary with fixed elevation

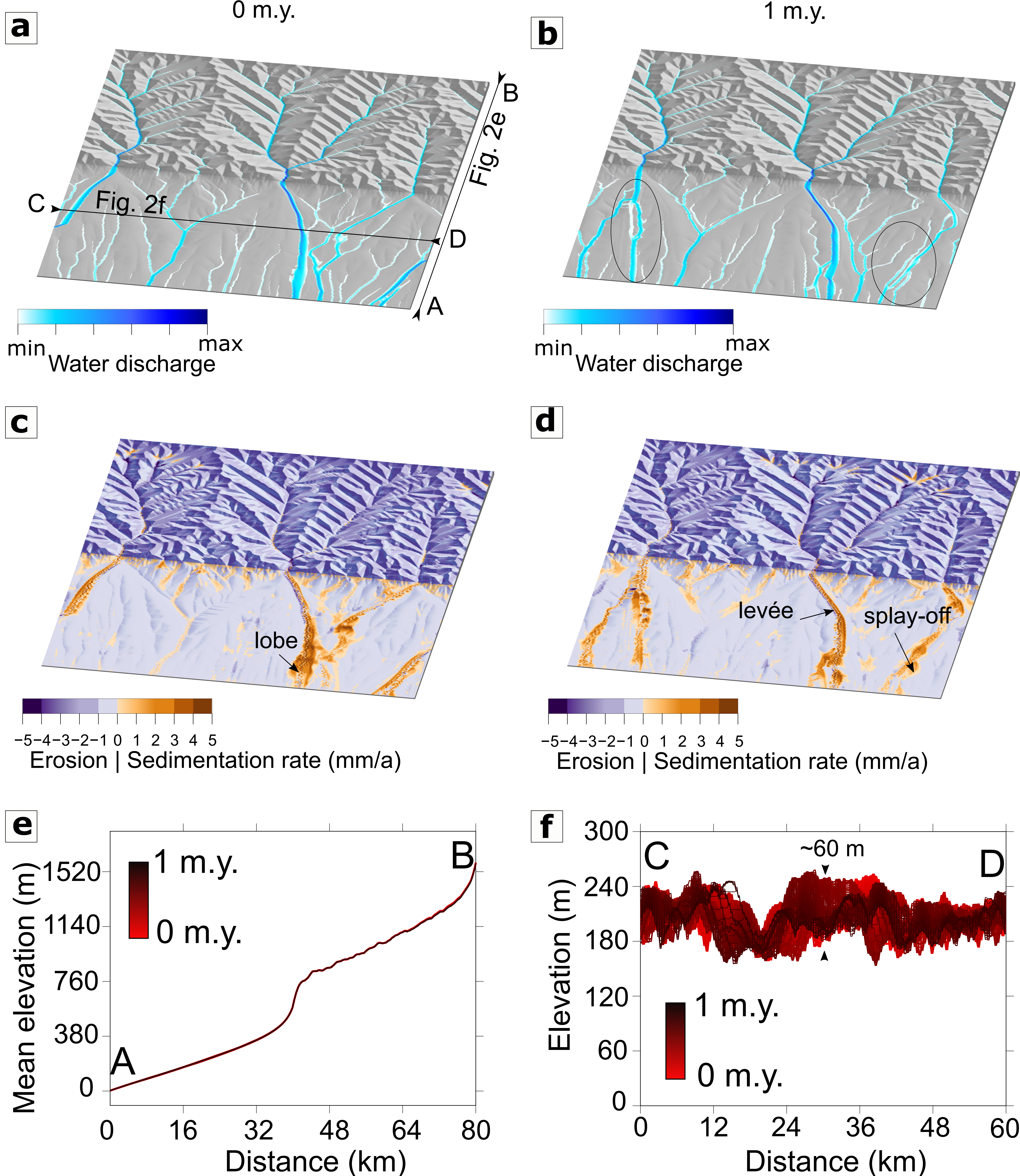

a
0 m.y.
b
1 m.y.
B
Fig. 2e
C
Fig. 2f
D
A
min
max
Water discharge
min
max
Water discharge
c
d
lobe
levée
splay-off
−5 −4 −3 −2 −1 0 1 2 3 4 5
Erosion | Sedimentation rate (mm/a)
−5 −4 −3 −2 −1 0 1 2 3 4 5
Erosion | Sedimentation rate (mm/a)
e
Mean elevation (m)
1520
1140
760
380
0
1 m.y.
0 m.y.
A
B
0 16 32 48 64 80
Distance (km)
f
Elevation (m)
300
240
180
120
60
0
C
D
~60 m
1 m.y.
0 m.y.
0 12 24 36 48 60
Distance (km)

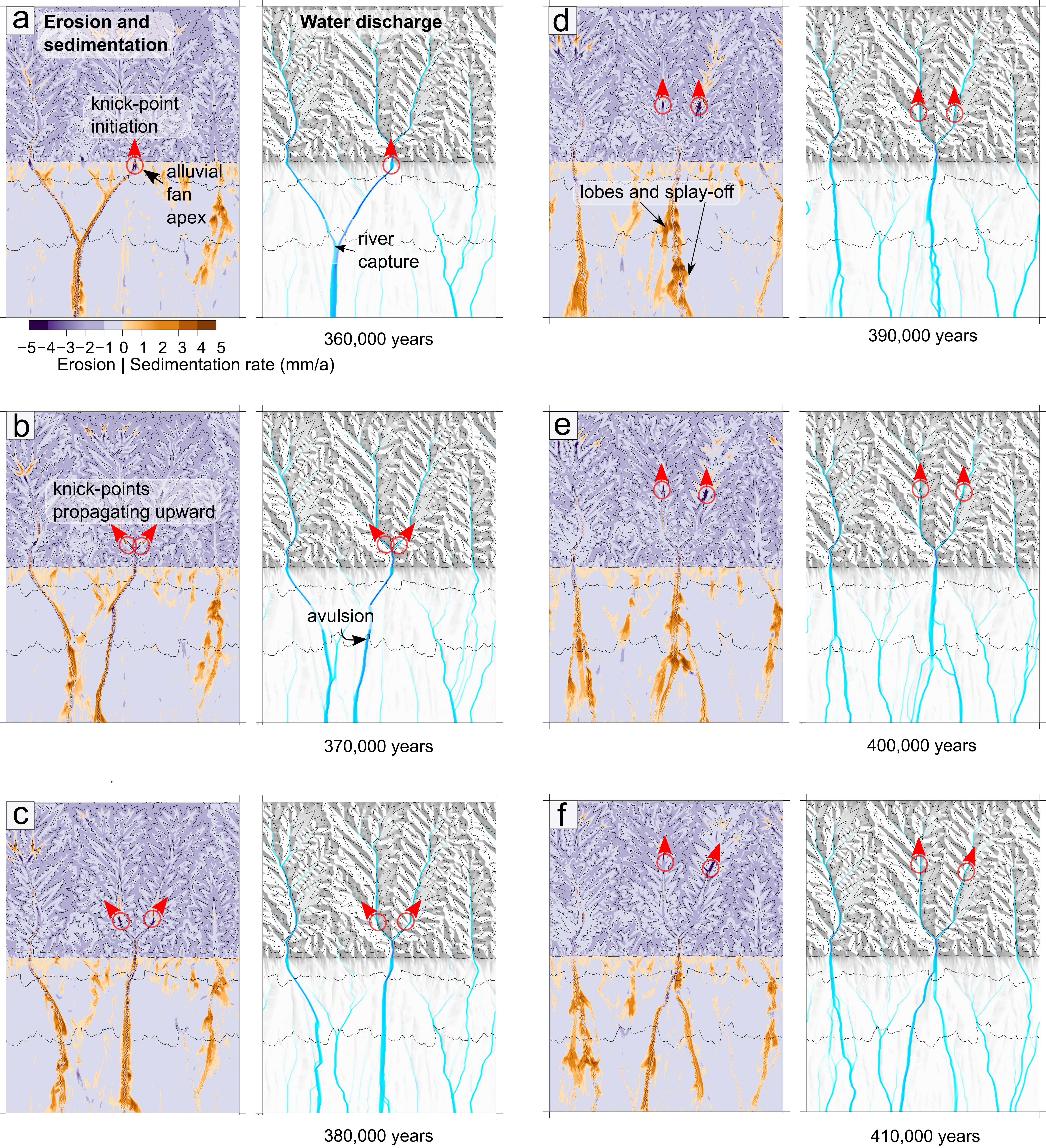

a
Erosion and sedimentation
Water discharge
knick-point initiation
alluvial fan apex
river capture
−5 −4 −3 −2 −1 0 1 2 3 4 5
Erosion | Sedimentation rate (mm/a)
360,000 years
b
knick-points propagating upward
avulsion
370,000 years
c
380,000 years
d
lobes and splay-off
390,000 years
e
400,000 years
f
410,000 years

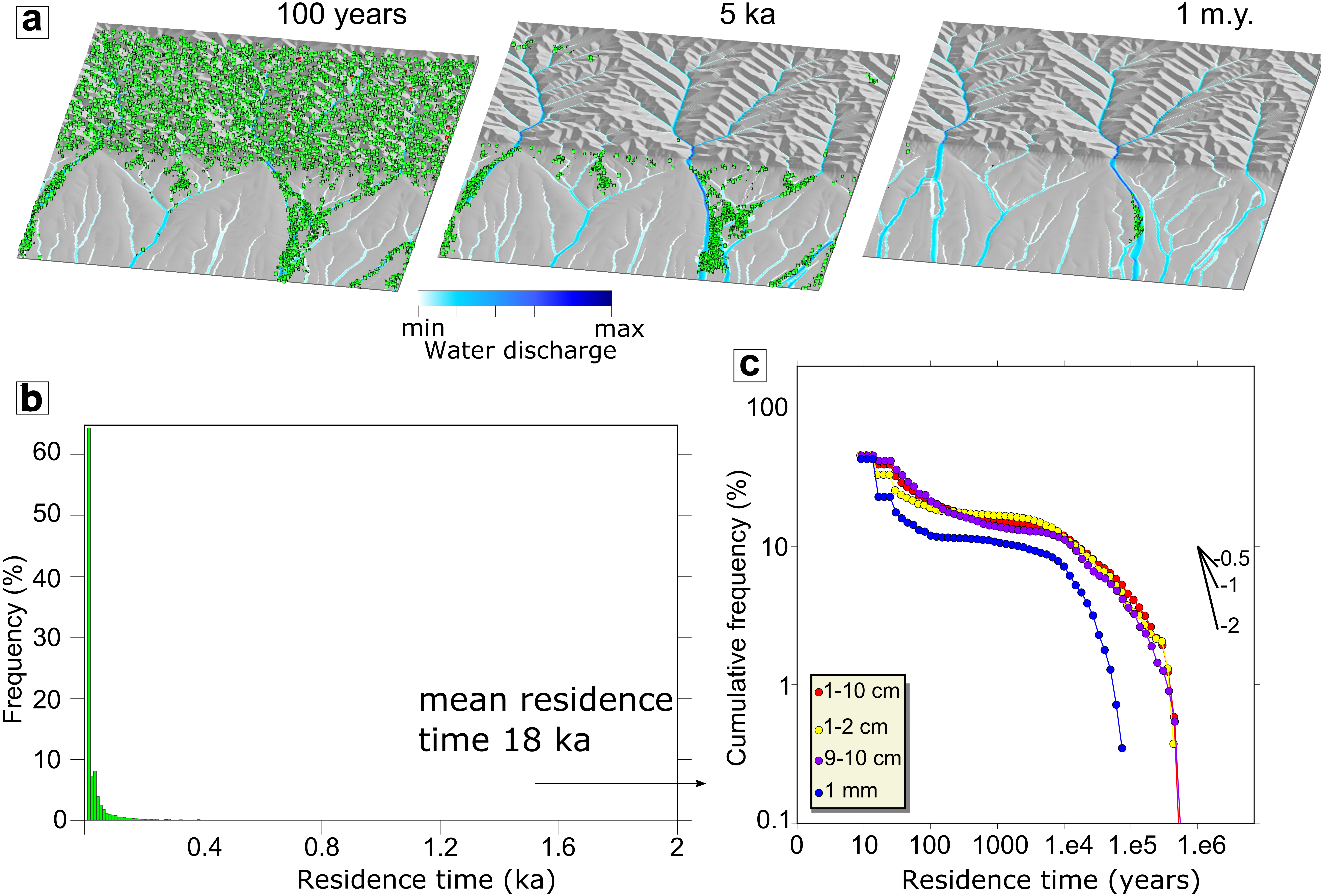
a
100 years
5 ka
1 m.y.
min
max
Water discharge
b
Frequency (%)
60
50
40
30
20
10
0
0.4
0.8
1.2
1.6
2
Residence time (ka)
mean residence time 18 ka
c
Cumulative frequency (%)
100
10
1
0.1
0
10
100
1000
1.e4
1.e5
1.e6
Residence time (years)
-0.5
-1
-2
1-10 cm
1-2 cm
9-10 cm
1 mm

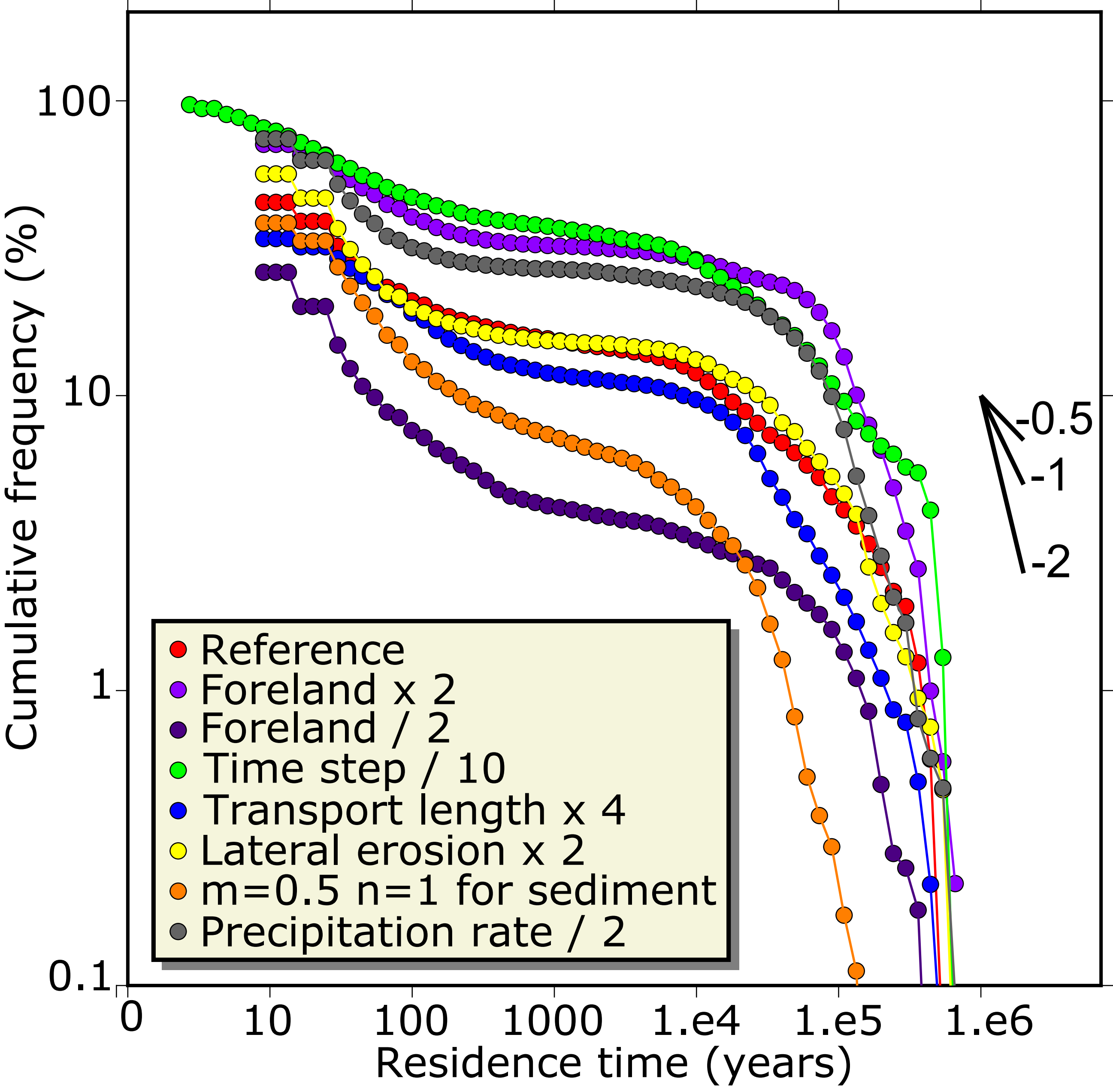

100
10
1
0.1
Cumulative frequency (%)
0
10
100
1000
1.e4
1.e5
1.e6
Residence time (years)
-0.5
-1
-2
Reference
Foreland x 2
Foreland / 2
Time step / 10
Transport length x 4
Lateral erosion x 2
m=0.5 n=1 for sediment
Precipitation rate / 2

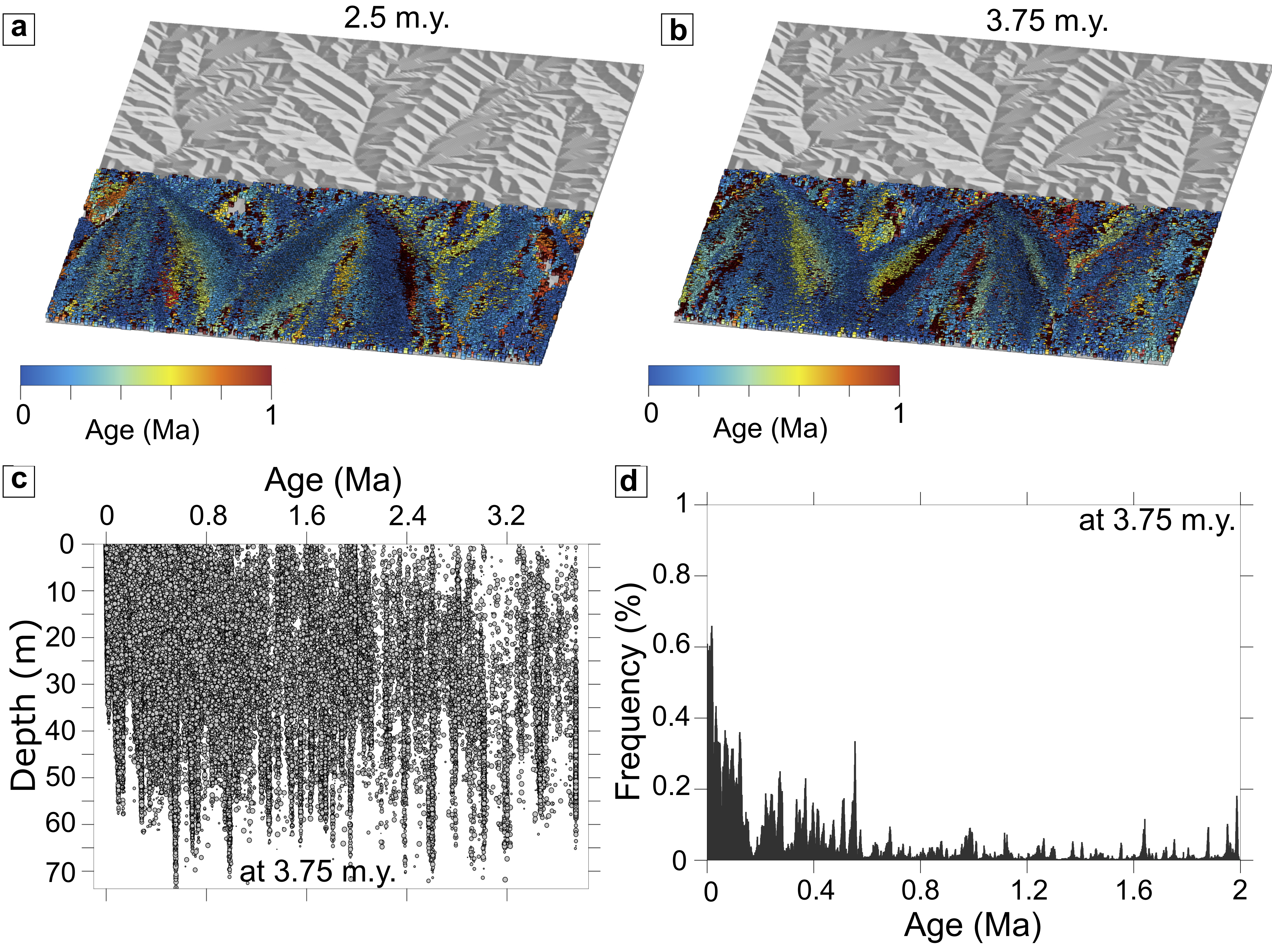
a
2.5 m.y.
0
Age (Ma)
1
b
3.75 m.y.
0
Age (Ma)
1
c
Age (Ma)
0
0.8
1.6
2.4
3.2
Depth (m)
0
10
20
30
40
50
60
70
at 3.75 m.y.
d
Frequency (%)
1
0.8
0.6
0.4
0.2
0
at 3.75 m.y.
0
0.4
0.8
1.2
1.6
2
Age (Ma)

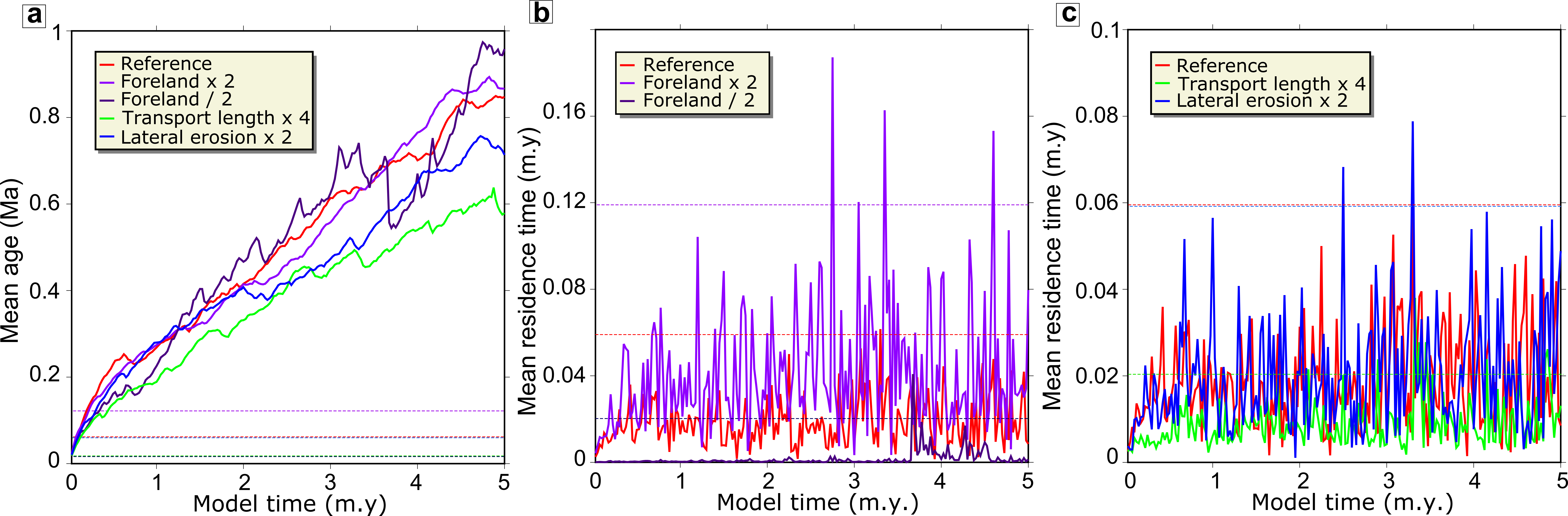
a
Reference
Foreland x 2
Foreland / 2
Transport length x 4
Lateral erosion x 2
Mean age (Ma)
Model time (m.y)
0
0.2
0.4
0.6
0.8
1
0
1
2
3
4
5
b
Reference
Foreland x 2
Foreland / 2
Mean residence time (m.y)
Model time (m.y.)
0
0.04
0.08
0.12
0.16
c
Reference
Transport length x 4
Lateral erosion x 2
Mean residence time (m.y)
Model time (m.y.)
0
0.02
0.04
0.06
0.08
0.1

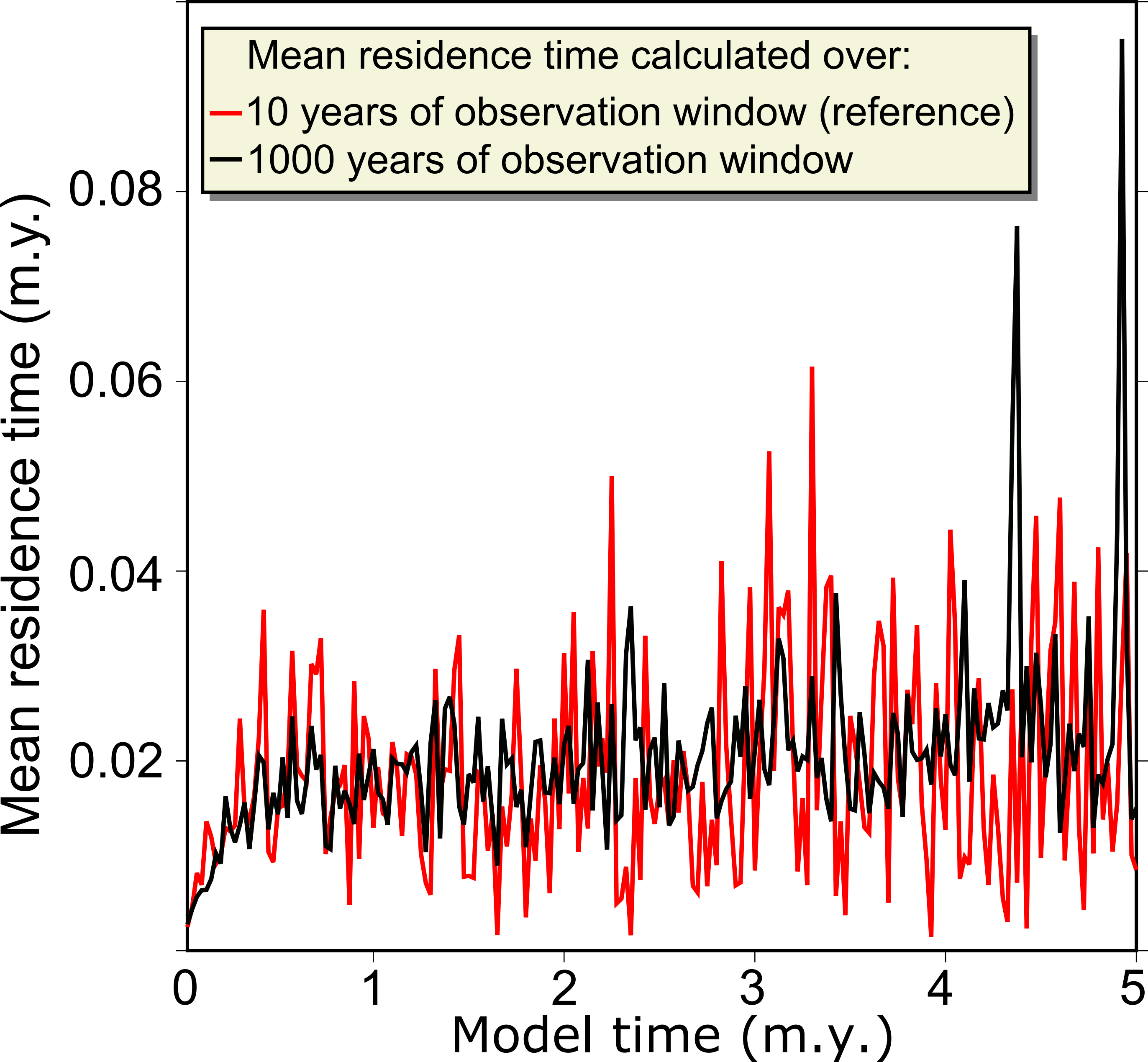
Mean residence time calculated over:
10 years of observation window (reference)
1000 years of observation window
0.08
0.06
0.04
0.02
Mean residence time (m.y.)
0
1
2
3
4
5
Model time (m.y.)

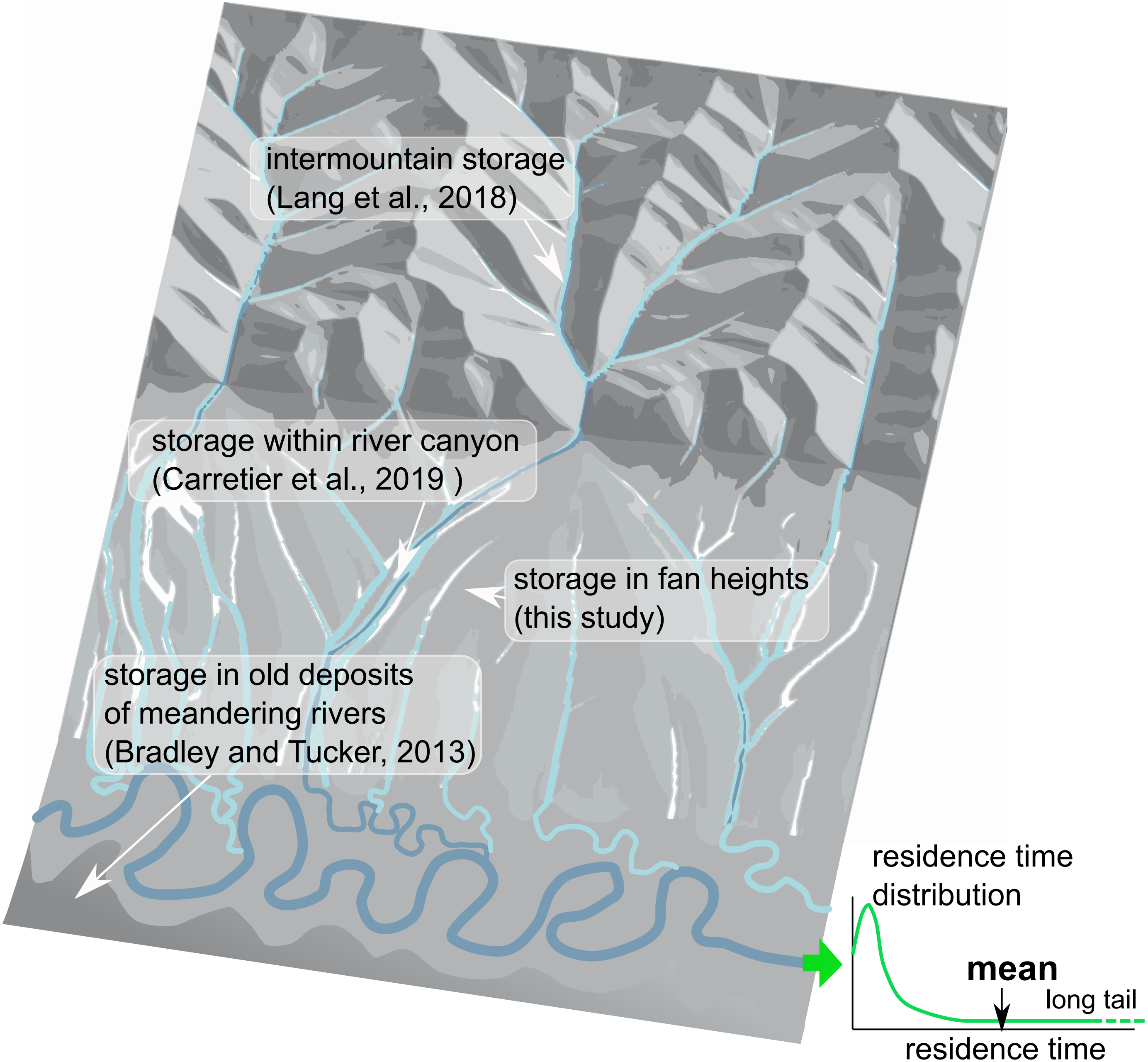

intermountain storage
(Lang et al., 2018)
storage within river canyon
(Carretier et al., 2019)
storage in fan heights
(this study)
storage in old deposits
of meandering rivers
(Bradley and Tucker, 2013)
residence time
distribution
mean
long tail
residence time